

Probing Modified Gravity with Integrated Sachs-Wolfe CMB and Galaxy Cross-correlations

Joshua A. Kable¹, Giampaolo Benevento¹, Noemi Frusciante², Antonio De Felice³, Shinji Tsujikawa⁴

¹*Johns Hopkins University 3400 North Charles Street Baltimore, MD 21218, USA*

²*Instituto de Astrofísica e Ciências do Espaço, Faculdade de Ciências da Universidade de Lisboa, Edifício C8, Campo Grande, P-1749016, Lisboa, Portugal*

³*Center for Gravitational Physics, Yukawa Institute for Theoretical Physics, Kyoto University, 606-8502, Kyoto, Japan*

⁴*Department of Physics, Waseda University, 3-4-1 Okubo, Shinjuku, Tokyo 169-8555, Japan*

(Dated: September 7, 2022)

We use the cross-correlation power spectrum of the integrated Sachs-Wolfe (ISW) effect in the cosmic microwave background (CMB) temperature anisotropy and galaxy fluctuations to probe the physics of late-time cosmic acceleration. For this purpose, we focus on three models of dark energy that belong to a sub-class of Horndeski theories with the speed of gravity equivalent to that of light: Galileon Ghost Condensate (GGC), Generalized Cubic Covariant Galileon (GCCG), and K-mouflage. In the GGC and GCCG models, the existence of cubic-order scalar self-interactions allows a possibility for realizing negative ISW-galaxy cross-correlations, while the K-mouflage model predicts a positive correlation similar to the Λ -cold-dark-matter (Λ CDM) model. In our analysis, we fix the parameters of each model to their best-fit values derived from a baseline likelihood analysis with observational data from CMB, baryon acoustic oscillations, and supernovae type Ia. Then we fit those best-fit models to the ISW-galaxy cross-correlation power spectrum extracted from a collection of photometric redshift surveys. We find that both GGC and GCCG best-fit models degrade the fit to the ISW-galaxy cross-correlation data compared to Λ CDM best-fit model. This is attributed to the fact that, for their best-fit values constrained from the baseline likelihood, the cubic-order scalar self-interaction gives rise to suppressed ISW tails relative to Λ CDM. The K-mouflage best-fit model is largely degenerate with the Λ CDM best-fit model and has a positively correlated ISW-galaxy power close to that of Λ CDM.

CONTENTS

I. Introduction	2
II. ISW-galaxy cross-correlations	3
III. Dark energy models	6
A. Shift-symmetric Horndeski theories	6
1. Galileon Ghost Condensate (GGC)	8
2. Generalized Cubic Covariant Galileon (GCCG)	10
B. K-mouflage	12
IV. Methodology and Data	14
A. Einstein-Boltzmann code	14
B. The significance of the ISW	14
C. Best-fit values for cosmological and model parameters	16
V. Results and Discussion	16
A. Galileon Ghost Condensate (GGC)	18
B. Generalized Cubic Covariant Galileon (GCCG)	19
C. K-mouflage	21
VI. Conclusion	22
Acknowledgments	23
References	23

I. INTRODUCTION

The observations of supernovae type Ia (SNIa) [1, 2], along with the measurements of the cosmic microwave background (CMB) [3, 4], and the baryon acoustic oscillations (BAO) [5], have shown that the universe is currently undergoing an epoch of cosmic acceleration. The unknown source for this phenomenon is dubbed dark energy, which has an effective negative pressure P against gravity. At the background level dark energy is quantified by an equation of state parameter $w_{\text{DE}} = P/\rho$, where ρ is a dark energy density. The simplest model of dark energy is the cosmological constant given by the constant density $\rho = \Lambda$ [6–8], in which case the equation of state parameter is $w_{\text{DE}} = -1$. The standard model of cosmology, Λ CDM, is built on the framework of General Relativity (GR) and assumes a homogeneous and isotropic background with a cosmological constant, Λ , and a non-relativistic cold dark matter (CDM) fluid. With these simple assumptions, the Λ CDM model has been overall successful at explaining observational data over a vast array of cosmological epochs (see e.g., [9–12]).

Despite this success, if the vacuum energy appearing in particle physics is responsible for the cosmological constant, the typical vacuum energy scale is enormously higher than the observed dark energy scale (see e.g., [6, 13–15] for reviews). Moreover, there are currently tensions on the values of some cosmological parameters between different data sets. The tension on the value of today’s cosmic expansion rate $H_0 = 100 h \text{ km sec}^{-1} \text{ Mpc}^{-1}$ in the Λ CDM model is estimated to be $\sim 4\sigma$ between the Planck CMB observations and its direct measurements at low redshifts [16, 17] (see Refs. [18, 19] for reviews). Similarly, there is a $2\sim 3\sigma$ tension for the determination of the amount of galaxy clustering quantified by the parameter $S_8 \equiv \sigma_{8,0} \sqrt{\Omega_{\text{m},0}}/0.3$, where $\sigma_{8,0}$ is present-day amplitude of matter fluctuations on scale $8h^{-1} \text{ Mpc}$ and $\Omega_{\text{m},0}$ is today’s density parameter of nonrelativistic matter [20–24].

There have been many dark energy models proposed so far designed to improve the aforementioned problems in Λ CDM (see e.g., [25–27] for reviews). One simple extension is to consider time variations in the dark energy equation of state. For instance, the quintessence scenario based on a scalar field slowly rolling on a nearly flat potential gives rise to time variation of w_{DE} in the region $w_{\text{DE}} > -1$ [28–30]. However, there has been no strong statistical evidence that quintessence models are observationally favored over Λ CDM [31, 32]. Moreover, it has been shown that the quintessence parameter space $w_{\text{DE}} > -1$ is expected to prefer a lower value of H_0 meaning it would worsen the Hubble tension (See e.g. Ref. [33]).

Alternatively, one can consider cosmological models that exhibit deviations from GR on scales relevant to the present-day cosmic acceleration. From Lovelock’s theorem [34, 35], any infrared departure from GR should include new degrees of freedom (DOFs). The new DOFs can be a scalar field, a vector field, or a massive graviton. Among them, the scalar field is the simplest example that is compatible with the cosmological dynamics of the homogeneous and isotropic background. In so-called scalar-tensor theories where the scalar field is coupled to gravity through nonminimal and derivative couplings, there have been numerous attempts for constructing viable modified gravity (MG) models of late-time cosmic acceleration [14, 28, 36–52]. Unlike quintessence, it is possible to realize the phantom dark energy equation of state ($w_{\text{DE}} < -1$) without having ghosts. Many of such models belong to a framework of Horndeski theories [53] in which the Lagrangian is constructed to include the gravitational and scalar-field equations of motion up to second-order derivatives (see also Refs. [54–56]).

After the gravitational-wave event GW170817 [57], the speed of gravitational waves c_t is constrained to be very close to that of light c . The Lagrangian of Horndeski theories realizing $c_t = c$ is restricted to be of the form $L = G_2(\phi, X) + G_3(\phi, X)\square\phi + G_4(\phi)R$ [55, 58], where R is the Ricci scalar, G_4 is a function of the scalar field ϕ , and G_2 and G_3 depend on ϕ as well as $X = \nabla^\mu\phi\nabla_\mu\phi$ (with ∇^μ being the covariant derivative operator). Even in this subclass of Horndeski theories, there are several models of dark energy showing a better fit to the SNIa, CMB, and BAO data in comparison to Λ CDM.

One of such examples is the Galileon Ghost Condensate (GGC) model [48, 59] characterized by the functions $G_2(X) = a_1X + a_2X^2$, $G_3(X) = 3a_3X$, and $G_4(X) = M_{\text{pl}}^2/2$, where M_{pl} is the reduced Planck mass. This includes the Cubic Galileon (G3) [60] as a specific case ($a_2 = 0$), which is disfavored by data [61–63] mostly due to the large deviation of w_{DE} from -1 for a tracker solution ($w_{\text{DE}} = -2$ during the matter era). The existence of the term a_2X^2 in the GGC model allows a phantom dark energy equation of state between -2 and -1 . The large-scale CMB temperature anisotropy can be suppressed by the cubic interaction term $3a_3X\square\phi$ relative to Λ CDM. These properties lead to a statistical preference of GGC over Λ CDM, when the SNIa, CMB, and BAO data are used in the analysis [64]. A similar statistical preference [65] is also present in the Generalized Cubic Covariant Galileon (GCCG) model [58, 66] characterized by the functions $G_2(X) = -c_2M_2^{4(1-p)}(-X/2)^p$, $G_3(X) = -c_3M_3^{1-4p_3}(-X/2)^{p_3}$, and $G_4 = M_{\text{pl}}^2/2$, which also realizes the phantom dark energy equation of state.

There are also dark energy models in which the scalar field has a nonminimal coupling $G_4(\phi)R$ to the Ricci scalar. One of such examples is K-mouflage [67–69], where the corresponding Lagrangian in the Jordan frame is of the form $L = G_2(\phi, X) + G_4(\phi)R$. The nonminimal coupling gives rise to the propagation of an effective fifth force between the scalar field and baryons [14], so it is necessary to implement a screening mechanism to hide the extra force in

local regions of the universe. Unlike the chameleon mechanism [70] or Vainshtein mechanism [71] in which a scalar potential $V(\phi)$ or a scalar self-interaction $G_3(X)\Box\phi$ suppresses the effective fifth force in the region of high densities, K-mouflage resorts to nonlinear kinetic terms in $G_2(X)$ for the screening mechanism to work. On today's Hubble scales, such nonlinear kinetic terms can drive cosmic acceleration as in the K-essence scenario [72, 73].

On scales relevant to the linear growth of large-scale structures, the presence of Lagrangians $G_3(X)\Box\phi$ and $G_4(\phi)R$ gives rise to an effective gravitational coupling G_{eff} with matter different from the Newton gravitational constant G_N [74, 75] (see also Refs. [76–79]). Then, the growth of matter density contrast is modified from that in Λ CDM, whose property can be used to place constraints on MG models from the growth rate measurements like redshift-space distortions (RSDs).

In MG models, the two gravitational potentials Ψ and Φ , which appear as the temporal and spatial components of metric perturbations in the longitudinal gauge, are not generally equivalent to each other. Thus, the relation between the lensing potential $\Phi_{\text{eff}} = \Psi + \Phi$ and the density contrast δ_m is subject to modification in comparison to Λ CDM [76–79]. As such, the MG models not only affect the weak lensing potential [80, 81] but also modify the low-multipole CMB temperature anisotropy through the integrated Sachs-Wolfe (ISW) effect [82, 83]. As a combined effect, the cross-correlation between the ISW effect in CMB and large-scale structure (LSS) [84] is affected as well. The ISW signal appears in the CMB power spectrum at large angular scales corresponding to multipoles $l \lesssim 40$, where the primary Sachs-Wolfe effect and cosmic variance are the dominant sources of anisotropy. This prevents the detection of the ISW signal using CMB data alone. However, such a signal can be isolated by cross-correlating the CMB data with LSS tracers [85–87]. This provides a powerful tool to constrain MG models of dark energy [62, 65, 88–91].

In this paper, we are interested in constraining the ISW effect due to modified gravitational interactions through the cross-correlation between CMB and galaxy surveys. To construct an ISW-galaxy cross-correlation likelihood, we extend to MG models the tomographic analysis of the ISW signal using photometric measurements of the redshift of galaxies applied to the Λ CDM model (see e.g., [87, 92–96]). We specialize our analysis to three the MG models mentioned above, i.e., GGC, GCCG, and K-mouflage. We show that the best-fit parameters in the GGC and GCCG models constrained by the SNIa, CMB, and BAO data give rise to a suppressed ISW power induced by the cubic interaction $G_3(X)\Box\phi$. This leads to worse fits to the ISW-galaxy cross-correlation data obtained from a collection of photometric redshift surveys that were originally combined in Ref. [87] for an ISW analysis assuming Λ CDM. Hence the ISW-galaxy cross-correlation power spectrum provides strong constraints on dark energy models containing the cubic derivative interaction $G_3(X)\Box\phi$. The best-fit parameters for K-mouflage are found to be largely degenerate with the Λ CDM case, meaning that we essentially recover the Λ CDM limit.

This paper is organized as follows. In Sec. II, we provide a review of the cross-correlation power spectrum between the ISW effect in CMB and galaxy clusterings. In Sec. III, we briefly revisit the dynamics of the background and perturbations in GGC, GCCG, and K-mouflage models. In Sec. IV, we outline the methodology adopted to probe our MG models with the ISW-galaxy cross-correlation power spectrum. In Sec. V, we present and discuss the results of our analysis for each model. Finally, in Sec. VI, we offer conclusions. Throughout the paper, we use the natural units where the speed of light c and the reduced Planck constant \hbar are equivalent to 1.

II. ISW-GALAXY CROSS-CORRELATIONS

We first review the power spectrum of ISW-galaxy cross-correlations in MG theories. This general prescription accommodates not only dark energy models in GR [84], but also those in scalar-tensor [97] and vector-tensor theories [98]. Let us consider the perturbed line element on the spatially flat Friedmann-Lemaître-Robertson-Walker (FLRW) background in the Newtonian gauge:

$$ds^2 = -(1 + 2\Psi) dt^2 + a^2(t) (1 - 2\Phi) \delta_{ij} dx^i dx^j, \quad (2.1)$$

where Ψ and Φ are the gravitational potentials that depend on time t and spatial position x^i , and $a(t)$ is the time-dependent scale factor.

The effective gravitational potentials associated with the bending of light rays is given by

$$\Phi_{\text{eff}} = \Psi + \Phi. \quad (2.2)$$

The ISW effect of CMB temperature anisotropy occurs by the time variation of Φ_{eff} after the recombination epoch. The ISW contribution δT_{ISW} to the CMB temperature perturbation divided by its average temperature \bar{T} can be quantified as

$$\frac{\delta T_{\text{ISW}}(\hat{n})}{\bar{T}} = - \int_0^{z_*} dz e^{-\tau(z)} \frac{\partial \Phi_{\text{eff}}}{\partial z}(z, \hat{n}\chi(z)), \quad (2.3)$$

where \hat{n} is a unit vector along the line of sight, and $z = 1/a - 1$ is the redshift with the value z_* at recombination, and τ is the visibility function.

The fluctuations of the angular distribution of galaxies, with the average number \bar{N}_g , are expressed in the form

$$\frac{\delta N_g(\hat{n})}{\bar{N}_g} = \int_0^{z_*} dz \delta_g(z, x^i) W(z), \quad (2.4)$$

where $W(z)$ is the selection function of the survey, and δ_g is the galaxy number density contrast. We relate δ_g with the matter density contrast δ_m , as

$$\delta_g(z, x^i) = b \delta_m(z, \hat{n} \chi(z)), \quad (2.5)$$

where b is a bias factor, and $\chi(z) = \int_0^z d\tilde{z}/H(\tilde{z})$ is a comoving distance. The selection function $W(z)$, which satisfies the normalization $\int_0^\infty dz W(z) = 1$, is specific of the galaxy survey considered. The typical choice of $W(z)$ approximating observed galaxy distributions is given by

$$W(z) = \frac{\beta}{\Gamma[(\alpha + 1)/\beta]} \left(\frac{z}{z_0}\right)^\alpha \exp\left[-\left(\frac{z}{z_0}\right)^\beta\right], \quad (2.6)$$

where $\Gamma[x]$ is the gamma function and α, β, z_0 are positive constants. For instance, the 2MASS and SDSS galaxy catalogues can be fitted by Eqn. (2.6) with the constants $(z_0, \alpha, \beta) = (0.072, 1.901, 1.752)$ and $(z_0, \alpha, \beta) = (0.113, 3.457, 1.197)$, respectively [84].

We expand the perturbations (2.3) and (2.4) in terms of the spherical harmonics $Y_{lm}(\hat{n})$, as

$$\frac{\delta T_{\text{ISW}}(\hat{n})}{\bar{T}} = \int_0^{z_*} dz \frac{\delta T_{\text{ISW}}}{\bar{T}}(z, \chi \hat{n}) = \sum_{l,m} a_{lm}^{\text{ISW}} Y_{lm}(\hat{n}), \quad (2.7)$$

$$\frac{\delta N_g(\hat{n})}{\bar{N}_g} = \int_0^{z_*} dz \frac{\delta N_g}{\bar{N}_g}(z, \chi \hat{n}) = \sum_{l,m} a_{lm}^g Y_{lm}(\hat{n}), \quad (2.8)$$

where $a_{lm}^{\text{ISW}} = \int d\Omega (\delta T_{\text{ISW}}(\hat{n})/\bar{T}) Y_{lm}^*(\hat{n})$ and $a_{lm}^g = \int d\Omega (\delta N_g(\hat{n})/\bar{N}_g) Y_{lm}^*(\hat{n})$, with Ω being a solid angle. We also expand $\delta T_{\text{ISW}}(z, \chi \hat{n})/\bar{T}$ and $\delta N_g(z, \chi \hat{n})/\bar{N}_g$ in terms of the Fourier series, respectively, as

$$\frac{\delta T_{\text{ISW}}}{\bar{T}}(z, \chi \hat{n}) = \int \frac{d^3 k}{(2\pi)^3} \frac{\delta T_{\text{ISW}}}{\bar{T}}(z, \mathbf{k}) e^{i\mathbf{k} \cdot \chi \hat{n}}, \quad \frac{\delta N_g}{\bar{N}_g}(z, \chi \hat{n}) = \int \frac{d^3 k}{(2\pi)^3} \frac{\delta N_g}{\bar{N}_g}(z, \mathbf{k}) e^{i\mathbf{k} \cdot \chi \hat{n}}, \quad (2.9)$$

where \mathbf{k} is a comoving wavenumber, with $k = |\mathbf{k}|$. Using the property $\int d\Omega e^{i\mathbf{k} \cdot \mathbf{r}} Y_{lm}^*(\hat{r}) = 4\pi i^l j_l(kr) Y_{lm}^*(\hat{k})$, where $j_l(kr)$ is a spherical Bessel function with the notations $\hat{r} = \mathbf{r}/r$ and $\hat{k} = \mathbf{k}/k$, the coefficients a_{lm}^{ISW} and a_{lm}^g reduce, respectively, to

$$a_{lm}^{\text{ISW}} = -\frac{i^l}{2\pi^2} \int_0^{z_*} dz_1 \int d^3 k_1 e^{-\tau(z_1)} \frac{\partial \Phi_{\text{eff}}}{\partial z}(z_1, k_1) j_l(k_1 \chi(z_1)) Y_{lm}^*(\hat{k}_1), \quad (2.10)$$

$$a_{lm}^g = \frac{i^l}{2\pi^2} \int_0^{z_*} dz_2 \int d^3 k_2 b W(z_2) \delta_m(z_2, k_2) j_l(k_2 \chi(z_2)) Y_{lm}^*(\hat{k}_2). \quad (2.11)$$

The cross-correlation between the ISW and galaxy fluctuations is expressed as

$$\left\langle \frac{\delta T_{\text{ISW}}(\hat{n}_1)}{\bar{T}} \frac{\delta N_g(\hat{n}_2)}{\bar{N}_g} \right\rangle = \sum_{l=2}^{\infty} \frac{2l+1}{4\pi} C_l^{\text{Tg}} \mathcal{P}_l(\cos \theta), \quad (2.12)$$

where \mathcal{P}_l is the Legendre polynomial with the angle θ between the unit vectors \hat{n}_1 and \hat{n}_2 , and C_l^{Tg} is the ISW-galaxy cross-correlation amplitude given by

$$C_l^{\text{Tg}} = \langle a_{lm}^{\text{ISW}} (a_{lm}^g)^* \rangle. \quad (2.13)$$

It is also useful to define the galaxy auto-correlation function as

$$\left\langle \frac{\delta N_g(\hat{n}_1)}{\bar{N}_g} \frac{\delta N_g(\hat{n}_2)}{\bar{N}_g} \right\rangle = \sum_{l=2}^{\infty} \frac{2l+1}{4\pi} C_l^{\text{gg}} \mathcal{P}_l(\cos \theta), \quad (2.14)$$

where

$$C_l^{\text{gg}} = \langle a_{lm}^g (a_{lm}^g)^* \rangle. \quad (2.15)$$

We consider the case in which the growth factor D of linear matter perturbations does not depend on the comoving wavenumber k . Indeed, this property holds for the MG models of dark energy discussed later in Sec. III on scales inside the sound horizon. Then, the matter density contrast is expressed in the form

$$\delta_m(z, \mathbf{k}) = D(z) \frac{\delta_m(0, \mathbf{k})}{D_0}, \quad (2.16)$$

where D_0 is today's value of D . Today's matter power spectrum P_m is defined by

$$\langle \delta_m(0, \mathbf{k}_1) \delta_m^*(0, \mathbf{k}_2) \rangle = (2\pi)^3 \delta_D^{(3)}(\mathbf{k}_1 - \mathbf{k}_2) P_m(k_1), \quad (2.17)$$

where $\delta_D^{(3)}$ is the three-dimensional delta function. We also introduce the quantity ψ_{ISW} characterizing the time variation of Φ_{eff} , as

$$\frac{\partial \Phi_{\text{eff}}}{\partial z} = -\psi_{\text{ISW}} \frac{\delta_m(0, \mathbf{k})}{D_0}. \quad (2.18)$$

Substituting Eqs. (2.10) and (2.11) into Eqn. (2.13), it follows that

$$C_l^{\text{Tg}} = \frac{2}{\pi} \int dk k^2 P_m(k) I_l^{\text{ISW}}(k) I_l^g(k), \quad (2.19)$$

where

$$I_l^{\text{ISW}}(k) = \int_0^{z_*} dz_1 e^{-\tau(z_1)} \frac{\psi_{\text{ISW}}(z, k)}{D_0} j_l(k\chi(z_1)), \quad (2.20)$$

$$I_l^g(k) = \int_0^{z_*} dz_2 b W(z_2) \frac{D(z)}{D_0} j_l(k\chi(z_2)). \quad (2.21)$$

Similarly, substituting Eqs. (2.10) and (2.11) into Eqn. (2.15) gives

$$C_l^{\text{gg}} = \frac{2}{\pi} \int dk k^2 P_m(k) I_l^g(k)^2. \quad (2.22)$$

The gravitational potentials Ψ and Φ are sourced by the matter density contrast δ_m through the perturbed Einstein equations. In Fourier space without the neutrino's anisotropic stress, the Poisson and lensing equations are given, respectively, by [76, 99, 100]

$$-k^2 \Psi = 4\pi G_N a^2 \mu(z, k) \rho_m \delta_m, \quad (2.23)$$

$$-k^2 \Phi_{\text{eff}} = 8\pi G_N a^2 \Sigma(z, k) \rho_m \delta_m, \quad (2.24)$$

where G_N is the Newton's gravitational constant, and the dimensionless quantities $\mu \equiv G_{\text{eff}}/G_N$ and Σ characterize the effective dimensionless gravitational couplings felt by matter and light, respectively. In terms of the gravitational slip parameter $\eta = \Phi/\Psi$, the relation between μ and Σ is

$$\Sigma = \frac{\eta + 1}{2} \mu. \quad (2.25)$$

The Λ CDM model gives $\mu = \Sigma = \eta = 1$. In MG theories, however, μ and Σ are generally different from 1. This leaves imprints for the growth-rate measurements as well as the ISW-galaxy cross-correlation power spectrum.

Let us consider the case in which the matter fields are minimally coupled to gravity. Then, the background nonrelativistic matter density evolves as

$$\rho_m = \rho_{m,0} (1+z)^3 = \frac{3H_0^2}{8\pi G_N} \Omega_{m,0} (1+z)^3 \quad (2.26)$$

where $\rho_{m,0}$ is today's value of ρ_m , and $\Omega_{m,0} = 8\pi G_N \rho_{m,0} / (3H_0^2)$. On using Eqs. (2.16), (2.24) and (2.26), it follows that

$$\Phi_{\text{eff}} = -\frac{3H_0^2 \Omega_{m,0}}{k^2} (1+z) D \Sigma \frac{\delta_m(0, \mathbf{k})}{D_0}. \quad (2.27)$$

Taking the z derivative of Eqn. (2.27) and comparing it with Eqn. (2.18), we can express ψ_{ISW} in the form

$$\psi_{\text{ISW}} = \frac{3H_0^2\Omega_{\text{m},0}}{k^2} D\Sigma\mathcal{F}, \quad (2.28)$$

where

$$\mathcal{F} \equiv 1 + (1+z) \frac{d}{dz} \ln(D\Sigma). \quad (2.29)$$

Substituting Eqn. (2.28) into Eqn. (2.19), the ISW-galaxy cross-correlation power spectrum yields

$$C_l^{\text{Tg}} = \frac{6H_0^2\Omega_{\text{m},0}}{\pi D_0^2} \int dk P_{\text{m}}(k) \int_0^{z_*} dz_1 e^{-\tau(z_1)} D\Sigma\mathcal{F} j_l(k\chi_1) \int_0^{z_*} dz_2 bW D j_l(k\chi_2), \quad (2.30)$$

where $\chi_i \equiv \chi(z_i)$ with $i = 1, 2$. For large values of k , we employ the Limber approximation for an arbitrary k -dependent function $f(k)$, i.e.,

$$\int dk k^2 f(k) j_l(k\chi_1) j_l(k\chi_2) \simeq \frac{\pi}{2} \frac{\delta(\chi_1 - \chi_2)}{\chi_1^2} f\left(\frac{l_{12}}{\chi_1}\right), \quad (2.31)$$

where $l_{12} \equiv l + 1/2$. Applying this approximation to Eqn. (2.30) together with the relation $dz/d\chi = H$, it follows that

$$C_l^{\text{Tg}} \simeq \frac{3H_0^2\Omega_{\text{m},0}}{D_0^2 l_{12}^2} \int_0^{z_*} dz e^{-\tau} H b D^2 \Sigma \mathcal{F} P_{\text{m}}\left(\frac{l_{12}}{\chi}\right). \quad (2.32)$$

The necessary condition for the negative ISW-galaxy cross-correlation ($C_l^{\text{Tg}} < 0$) to occur is quantified by

$$\mathcal{F} < 0. \quad (2.33)$$

In terms of the e-folding number $\mathcal{N} = \ln a = -\ln(1+z)$, the condition (2.33) can be expressed as

$$\mathcal{F} = 1 - \frac{D'(\mathcal{N})}{D(\mathcal{N})} - \frac{\Sigma'(\mathcal{N})}{\Sigma(\mathcal{N})} < 0. \quad (2.34)$$

Relating the growth rate D with the matter density parameter Ω_{m} and the growth index γ as $D'(\mathcal{N})/D(\mathcal{N}) = (\Omega_{\text{m}})^\gamma$, the term $D'(\mathcal{N})/D(\mathcal{N})$ is smaller than 1 for $0 < \Omega_{\text{m}} < 1$ and $0 < \gamma < 1$. Then, for the realization of the negative ISW-galaxy cross-correlation, it is at least necessary to satisfy the condition

$$\Sigma'(\mathcal{N}) > 0. \quad (2.35)$$

In GR we have $\Sigma = 1$ and hence $C_l^{\text{Tg}} > 0$. In MG theories, however, there are dark energy models in which Σ changes in time, so it is possible to realize the negative ISW-galaxy cross-correlation. In Sec. III, we will present such MG models of dark energy.

III. DARK ENERGY MODELS

In this section, we review dark energy models in the framework of cubic-order shift-symmetric Horndeski theories as well as K-mouflage theories. We first present the quantities μ and Σ derived under the quasi-static approximation in cubic-order Horndeski theories and apply them to GGC and GCCG models. We then proceed to the case of K-mouflage theories in which the nonminimal coupling $G_4(\phi)R$ is present besides the K-essence Lagrangian $G_2(\phi, X)$.

A. Shift-symmetric Horndeski theories

Let us consider cubic-order shift-symmetric Horndeski theories given by the action

$$\mathcal{S} = \int d^4x \sqrt{-g} \left[\frac{M_{\text{pl}}^2}{2} R + G_2(X) + G_3(X) \square\phi \right] + \mathcal{S}_{\text{m}}(\psi_{\text{m}}, g_{\mu\nu}), \quad (3.1)$$

where g is a determinant of the metric tensor $g_{\mu\nu}$, $M_{\text{pl}} = 1/\sqrt{8\pi G_{\text{N}}}$ is the reduced Planck mass, R is the Ricci scalar, and G_2, G_3 are functions of

$$X = \nabla^\mu \phi \nabla_\mu \phi, \quad (3.2)$$

with a scalar field ϕ . Since the action (3.1) does not contain the ϕ dependence in G_2 , the scalar field can be regarded as a massless field. This theory also gives the speed of gravity c_t equivalent to that of light [55, 58], so it evades the observational bound on the speed of gravitational waves [57].

The action \mathcal{S}_{m} corresponds to that of matter fields ψ_{m} . We will study the case in which the matter sector is described by perfect fluids minimally coupled to gravity. The background nonrelativistic (pressureless) matter density ρ_{m} on the FLRW background obeys

$$\dot{\rho}_{\text{m}} + 3H\rho_{\text{m}} = 0, \quad (3.3)$$

where $H = \dot{a}/a$ is the Hubble expansion rate, with a dot being the derivative with respect to t . The density ρ_{r} of radiation, which has the equation of state $w_{\text{r}} = 1/3$, satisfies the continuity equation $\dot{\rho}_{\text{r}} + 4H\rho_{\text{r}} = 0$. The background gravitational and scalar-field equations of motion are given by

$$3M_{\text{pl}}^2 H^2 = \rho_{\text{DE}} + \rho_{\text{m}} + \rho_{\text{r}}, \quad (3.4)$$

$$2M_{\text{pl}}^2 \dot{H} = -\rho_{\text{DE}} - P_{\text{DE}} - \rho_{\text{m}} - \frac{4}{3}\rho_{\text{r}}, \quad (3.5)$$

$$(G_{2,X} - 2\dot{\phi}^2 G_{2,XX} - 6H\dot{\phi}G_{3,X} + 6H\dot{\phi}^3 G_{3,XX})\ddot{\phi} + 3(HG_{2,X} - \dot{H}\dot{\phi}G_{3,X} - 3H^2\dot{\phi}G_{3,XX})\dot{\phi} = 0, \quad (3.6)$$

where

$$\rho_{\text{DE}} = -G_2 - 2\dot{\phi}^2 G_{2,X} + 6H\dot{\phi}^3 G_{3,X}, \quad (3.7)$$

$$P_{\text{DE}} = G_2 - 2\ddot{\phi}\dot{\phi}^2 G_{3,X}. \quad (3.8)$$

The dark energy equation of state is defined by

$$w_{\text{DE}} \equiv \frac{P_{\text{DE}}}{\rho_{\text{DE}}} = -\frac{G_2 - 2\ddot{\phi}\dot{\phi}^2 G_{3,X}}{G_2 + 2\dot{\phi}^2 G_{2,X} - 6H\dot{\phi}^3 G_{3,X}}. \quad (3.9)$$

From Eqn. (3.4), there is the constraint

$$\Omega_{\text{DE}} + \Omega_{\text{m}} + \Omega_{\text{r}} = 1, \quad (3.10)$$

where

$$\Omega_{\text{DE}} \equiv \frac{\rho_{\text{DE}}}{3M_{\text{pl}}^2 H^2}, \quad \Omega_{\text{m}} \equiv \frac{\rho_{\text{m}}}{3M_{\text{pl}}^2 H^2}, \quad \Omega_{\text{r}} \equiv \frac{\rho_{\text{r}}}{3M_{\text{pl}}^2 H^2}. \quad (3.11)$$

We also solve Eqs. (3.5) and (3.6) for \dot{H} and $\ddot{\phi}$ to know the dynamics of H and ϕ .

For the perturbations in the matter sector, we will consider the nonrelativistic matter perturbation $\delta\rho_{\text{m}}$ and velocity potential v in Fourier space, with the vanishing sound speed c_{m} . For the perturbed line element (2.1), their linear perturbation equations of motion are given by

$$\delta\dot{\rho}_{\text{m}} + 3H\delta\rho_{\text{m}} - 3\rho_{\text{m}}\dot{\Phi} + \frac{k^2}{a^2}\rho_{\text{m}}v = 0, \quad (3.12)$$

$$\dot{v} - \Psi = 0. \quad (3.13)$$

Taking the time derivative of Eqn. (3.12) and using Eqn. (3.13), the matter density contrast $\delta_{\text{m}} = \delta\rho_{\text{m}}/\rho_{\text{m}}$ obeys

$$\ddot{\delta}_{\text{m}} + 2H\dot{\delta}_{\text{m}} + \frac{k^2}{a^2}\Psi = 3\ddot{\Phi} + 6H\dot{\Phi}. \quad (3.14)$$

In order to derive an explicit relation between Ψ and δ_{m} , we need to resort to a so called quasi-static approximation (QSA) [36, 74, 101, 102]. For the modes inside the sound horizon, this amounts to picking up the terms containing δ_{m} and k^2/a^2 in the perturbation equations of motion arising from the gravity sector¹. The QSA was first exploited

¹ Within the Horndeski class of models, it has been proven to be a valid assumption for the wavenumber in the range $k > 10^{-3} h/\text{Mpc}$ [103, 104].

in full Horndeski theories in Ref. [74]. Under this approximation, Ψ and Φ_{eff} are related to δ_m through Eqs. (2.23) and (2.24), respectively, with [75]

$$\mu = \Sigma = 1 + \frac{4\dot{\phi}^4 G_{3,X}^2}{q_s c_s^2}, \quad (3.15)$$

where

$$q_s = 4M_{\text{pl}}^2 \left(-G_{2,X} + 2\dot{\phi}^2 G_{2,XX} + 6H\dot{\phi}G_{3,X} - 6H\dot{\phi}^3 G_{3,XX} \right) + 12\dot{\phi}^4 G_{3,X}^2, \quad (3.16)$$

$$c_s^2 = \frac{-4M_{\text{pl}}^2 (G_{2,X} - 2\ddot{\phi}G_{3,X} - 4H\dot{\phi}G_{3,X} + 2\ddot{\phi}\dot{\phi}^2 G_{3,XX}) - 4\dot{\phi}^4 G_{3,X}^2}{q_s}. \quad (3.17)$$

Under the QSA, the right hand-side of Eqn. (3.14) is negligible relative to its left hand-side, so using Eqn. (2.23) leads to

$$\ddot{\delta}_m + 2H\dot{\delta}_m - 4\pi G_N \mu \rho_m \delta_m \simeq 0. \quad (3.18)$$

The absence of scalar ghosts requires that

$$q_s > 0. \quad (3.19)$$

The quantity c_s^2 corresponds to the scalar sound speed squared in the sub-horizon limit. The Laplacian instability is absent for

$$c_s^2 > 0. \quad (3.20)$$

Under the conditions (3.19) and (3.20), both μ and Σ are larger than 1. Hence the gravitational interaction for linear perturbations inside the sound horizon ($c_s k > aH$) is stronger than that in the Λ CDM model. For the models of cosmic acceleration in which the cubic derivative interaction $G_3(X)$ contributes to the dark energy density, Σ grows at low redshifts. In such cases the condition (2.35) is satisfied, so there is a possibility for realizing the negative ISW-galaxy cross-correlation.

The property $\mu = \Sigma$ holds for the theories given by the Lagrangian $L = G_2(\phi, X) + G_3(\phi, X)\square\phi + (M_{\text{pl}}^2/2)R$, but Σ is different from μ in the presence of a nonminimal coupling $G_4(\phi)R$ [75]. For example, the theories with the Lagrangian $L = G_2(\phi, X) + G_4(\phi)R$, which include Brans-Dicke theories and $f(R)$ gravity as specific cases, lead to $\Sigma = M_{\text{pl}}^2/[2G_4(\phi)]$. If the scalar field does not vary much at late times, which is typically the case for dark energy models in the framework of Brans-Dicke theories and $f(R)$ gravity, the variation of Σ is not large enough to lead to the negative ISW-galaxy cross-correlation. As we will see in Sec. IIIB, K-mouflage belongs to this latter subclass of Horndeski theories.

1. Galileon Ghost Condensate (GGC)

As a first example within the framework of the action (3.1), we consider the GGC model characterized by the functions [48, 59]

$$G_2(X) = a_1 X + a_2 X^2, \quad G_3(X) = 3a_3 X, \quad (3.21)$$

where $a_{1,2,3}$ are constants. This model generalizes the Cubic Galileon model (hereafter G3) [60] by taking the term $a_2 X^2$ into account, which modifies the cosmic expansion and growth histories of both linear [48, 64] and non-linear [105] perturbations compared to G3. In particular, it works to suppress the large-scale CMB temperature anisotropy in comparison to the Λ CDM model. These features lead to the statistical preference of GGC over Λ CDM when data from CMB, BAO, SNIa, and RSDs are used [64]. Furthermore, the estimation of today's Hubble parameter H_0 constrained from CMB temperature and polarization data is consistent with its direct measurement at 2σ , alleviating the Hubble tension [64].

We introduce dimensionless variables to compute some relevant quantities for our analysis, which are defined by

$$x_1 = -\frac{a_1 \dot{\phi}^2}{3M_{\text{pl}}^2 H^2}, \quad x_2 = \frac{a_2 \dot{\phi}^4}{M_{\text{pl}}^2 H^2}, \quad x_3 = \frac{6a_3 \dot{\phi}^3}{M_{\text{pl}}^2 H}. \quad (3.22)$$

The Friedmann equation is given by Eqn. (3.4) with the dark energy density parameter

$$\Omega_{\text{DE}} = x_1 + x_2 + x_3. \quad (3.23)$$

Solving Eqs. (3.5) and (3.6) for $h \equiv \dot{H}/H^2$ and $\epsilon_\phi \equiv \dot{\phi}/(H\dot{\phi})$, it follows that

$$h = -\frac{12x_1^2 + 2(16x_2 + 12x_3 + 3\Omega_{\text{m}} + 4\Omega_{\text{r}})x_1 + 16x_2^2 + 4(6x_3 + 3\Omega_{\text{m}} + 4\Omega_{\text{r}})x_2 + (9x_3 + 6\Omega_{\text{m}} + 8\Omega_{\text{r}})x_3}{4x_1 + 8x_2 + 4x_3 + x_3^2}, \quad (3.24)$$

$$\epsilon_\phi = \frac{-12x_1 - 8x_2 + (6x_1 + 4x_2 + 3\Omega_{\text{m}} + 4\Omega_{\text{r}} - 6)x_3 + 3x_3^2}{4x_1 + 8x_2 + 4x_3 + x_3^2}. \quad (3.25)$$

The dark energy equation of state (3.9) yields

$$w_{\text{DE}} = \frac{3x_1 + x_2 - \epsilon_\phi x_3}{3(x_1 + x_2 + x_3)}. \quad (3.26)$$

Let us consider the case in which the cubic derivative interaction $G_3(X)$ dominates over $G_2(X)$ in the radiation- or matter-dominated epochs. Since the condition $\{|x_1|, |x_2|\} \ll |x_3| \ll 1$ is satisfied in this regime, Eqs. (3.24) and (3.25) give the approximate relations

$$h \simeq -\frac{1}{2}(3\Omega_{\text{m}} + 4\Omega_{\text{r}}), \quad \epsilon_\phi \simeq \frac{1}{4}(3\Omega_{\text{m}} + 4\Omega_{\text{r}} - 6). \quad (3.27)$$

Then, from Eqn. (3.26), we obtain

$$w_{\text{DE}} \simeq -\frac{1}{3}\epsilon_\phi \simeq \frac{1}{2} - \frac{1}{4}\Omega_{\text{m}} - \frac{1}{3}\Omega_{\text{r}}, \quad (3.28)$$

so that $w_{\text{DE}} \simeq 1/6$ in the radiation era and $w_{\text{DE}} \simeq 1/4$ in the matter era.

Since $|x_1|$ increases faster than $|x_3|$, it can happen that the solutions approach a tracker solution satisfying $H\dot{\phi} = \text{constant}$. This condition translates to $h = -\epsilon_\phi$, so that $x_3 = -2x_1$ for $x_2 \rightarrow 0$. Ignoring x_2 in comparison to x_1 and x_3 , the dark energy equation of state for the tracker yields

$$w_{\text{DE}} = -1 + \frac{2}{3}h, \quad (3.29)$$

so that $w_{\text{DE}} = -7/3$ during the radiation era and $w_{\text{DE}} = -2$ during the matter era. The moment at which the solutions approach the tracker depends on the initial conditions of x_1 , x_2 , and x_3 . The existence of nonvanishing x_2 works to prevent the solutions from approaching the tracker. Even when the tracker solution is not reached, it is possible to realize the phantom dark energy equation of state ($w_{\text{DE}} < -1$) without having ghosts [48, 64]. Finally, the cosmological trajectories converge to a de Sitter attractor ($w_{\text{DE}} = -1$, $\Omega_{\text{DE}} = 1$, $\Omega_{\text{m}} = 0$, $\Omega_{\text{r}} = 0$), at which the two relations $x_1 = -2 + x_3/2$ and $x_2 = 3 - 3x_3/2$ hold.

From Eqs. (3.16) and (3.17), the conditions for the absence of ghosts and Laplacian instabilities are given, respectively, by

$$q_s = \frac{3H^2 M_{\text{pl}}^4}{\dot{\phi}^2} (4x_1 + 8x_2 + 4x_3 + x_3^2) > 0, \quad (3.30)$$

$$c_s^2 = \frac{12x_1 + 8x_2 + 4(\epsilon_\phi + 2)x_3 - x_3^2}{3(4x_1 + 8x_2 + 4x_3 + x_3^2)} > 0. \quad (3.31)$$

In the regime characterized by $\{|x_1|, |x_2|\} \ll |x_3| \ll 1$, these two conditions are satisfied for $x_3 > 0$. On the tracker ($x_3 = -2x_1$ with $x_2 \rightarrow 0$), we require that $x_1 < 0$ for the consistency with (3.30) and (3.31). On the late-time de Sitter solution, the quantities (3.30) and (3.31) reduce, respectively, to

$$q_s = \frac{4H^2 M_{\text{pl}}^4}{3\dot{\phi}^2} (x_2^2 + 3x_2 + 18), \quad c_s^2 = \frac{x_2(3 - x_2)}{3(x_2^2 + 3x_2 + 18)}. \quad (3.32)$$

Hence we require the condition $0 < x_2 < 3$ for the stability of the de Sitter solution. We will consider the cosmological evolution in which $\dot{\phi}$ does not change the sign. Then, the signs of x_1 , x_2 , and x_3 consistent with the stability conditions are

$$x_1 < 0, \quad x_2 > 0, \quad x_3 > 0. \quad (3.33)$$

Today's values of x_1 , x_2 , and x_3 constrained by the observational data of CMB, BAO, SNIa, and RSD data do exist in this range [64].

From Eqn. (3.15), we have

$$\mu = \Sigma = 1 + \frac{x_3^2}{12x_1 + 8x_2 + 4(\epsilon_\phi + 2)x_3 - x_3^2}. \quad (3.34)$$

In the two early-time cosmological epochs discussed above, the right hand-side of Eqn. (3.34) reduces to

$$\mu = \Sigma \simeq \begin{cases} 1 + \frac{x_3}{2 + 3\Omega_m + 4\Omega_r} & \text{for } \{|x_1|, |x_2|\} \ll |x_3| \ll 1, \\ 1 + \frac{x_3}{2(1 + 3\Omega_m + 4\Omega_r)} & \text{for } x_3 = -2x_1, \quad x_2 \rightarrow 0. \end{cases} \quad (3.35)$$

With the growth of x_3 , Σ increases in time. The growth of Σ is particularly significant in the late universe at which x_3 contributes to the dark energy density. Hence it is possible to realize the negative ISW-galaxy cross-correlations in the GCC model.

2. Generalized Cubic Covariant Galileon (GCCG)

Let us consider the GCCG model [58] specified by the functions

$$G_2(X) = -c_2 M_2^{4(1-p)} (-X/2)^p, \quad G_3(X) = -c_3 M_3^{1-4p_3} (-X/2)^{p_3}, \quad (3.36)$$

where c_2 , c_3 , p , p_3 are dimensionless constants, and M_2 , M_3 are constants having a dimensionless of mass. Instead of p_3 , we will use the parameter q defined by

$$q = p_3 - p + \frac{1}{2}. \quad (3.37)$$

The GCCG model allows the existence of a tracker solution obeying the relation $H\dot{\phi}^{2q} = \text{constant}$ with $q > 0$. We note that the G3 model corresponds to the powers $p = 1$, $p_3 = 1$, and $q = 1/2$. In the following, we will consider the case of positive values of p and q , which are actually consistent with the stability conditions discussed below.

To study the cosmological dynamics, it is convenient to introduce the following dimensionless variables [58, 66]

$$x \equiv \frac{\dot{\phi}}{H M_{\text{pl}}}, \quad r_1 \equiv \left(\frac{x_{\text{dS}}}{x}\right)^{2q} \left(\frac{H_{\text{dS}}}{H}\right)^{1+2q}, \quad r_2 \equiv \left[\left(\frac{x}{x_{\text{dS}}}\right)^2 \frac{1}{r_1^3}\right]^{\frac{p+2q}{1+2q}}, \quad (3.38)$$

where x_{dS} and H_{dS} are the values of x and H on the late-time self-accelerating de Sitter solution, respectively (at which $\dot{\phi}$ and H are constants with $r_1 = 1$ and $r_2 = 1$). We will consider the solution in the range $x > 0$ without loss of generality.

We relate the masses M_2 and M_3 with H_{dS} , as

$$M_2 = (H_{\text{dS}} M_{\text{pl}})^{1/2}, \quad M_3 = \left(H_{\text{dS}}^{-2p_3} M_{\text{pl}}^{1-2p_3}\right)^{1/(1-4p_3)}. \quad (3.39)$$

Using Eqs. (3.4) and (3.5) on the de Sitter solution, the coefficients c_2 and c_3 are expressed as

$$c_2 = 3 \cdot 2^p x_{\text{dS}}^{-2p}, \quad c_3 = \frac{2^{p+q+1/2}}{2p+2q-1} p x_{\text{dS}}^{-2(p+q)}. \quad (3.40)$$

The density parameter and equation of state of dark energy are given, respectively, by

$$\Omega_{\text{DE}} = [2p - (2p-1)r_1] r_1^{1+\alpha} r_2, \quad (3.41)$$

$$w_{\text{DE}} = -\frac{(\Omega_r - 3 + 12r_1 - 6r_1^2)p + 3(2q-1)r_1 + 3r_1^2}{3[(2-2r_1 + r_1^{1+\alpha}r_2)p + 2q-1 + r_1][2p + (1-2p)r_1]}, \quad (3.42)$$

where

$$\alpha \equiv \frac{p+2q}{1+2q}. \quad (3.43)$$

For the derivation of Eqn. (3.42), we eliminated Ω_m by using Eqn. (3.10).

The variable r_1 obeys the differential equation

$$r_1'(\mathcal{N}) = \frac{r_1(r_1 - 1)[3 - 6p - 12q + (1 - 2p)\Omega_r - 3r_1^{2+\alpha}r_2 - 6p(1 - r_1)r_1^{1+\alpha}r_2]}{2p(2 - 2r_1 + r_1^{1+\alpha}r_2) - 2 + 4q + 2r_1}. \quad (3.44)$$

It is also straightforward to derive the differential equations for r_2 and Ω_r [58, 66]. In Eqn. (3.44), there are two kinds of fixed points characterized by $r_1 = 0$ and $r_1 = 1$. The tracker corresponds to the fixed point satisfying $r_1 = 1$ and $r_2 \ll 1$, whereas the de Sitter solution is characterized by $r_1 = 1$ and $r_2 = 1$. For the initial condition $r_1 \ll 1$, the quantity r_1 can grow to reach the tracker during the radiation or matter era. After the growth of r_2 toward 1, the solutions finally converge to the de Sitter fixed point.

From Eqn. (3.42), the dark energy equation of state in the regime $r_1 \ll 1$ and $r_2 \ll 1$ is approximately given by²

$$w_{\text{DE}} \simeq \frac{3 - \Omega_r}{12(p + q) - 6}. \quad (3.45)$$

For the G3 model ($p = 1$ and $q = 1/2$), this reduces to $w_{\text{DE}} \simeq 1/4 - \Omega_r/12$, whose value coincides with Eqn. (3.28) derived in the limit $\{|x_1|, |x_2|\} \ll |x_3| \ll 1$ in the GGC model.

On the tracker characterized by $r_1 = 1$ and $r_2 \ll 1$, the dark energy equation of state is given by

$$w_{\text{DE}} = -1 - \frac{1}{6}(3 + \Omega_r)s, \quad (3.46)$$

where

$$s \equiv \frac{p}{q}. \quad (3.47)$$

The quantity s characterizes the deviation from the Λ CDM model³. For positive values of p and q , the phantom tracker equation of state can be realized. Finally, the solutions approach the de Sitter attractor ($r_1 = r_2 = 1$) with $w_{\text{DE}} = -1$.

For the quantities associated with perturbations, we have

$$\tilde{q}_s \equiv \frac{q_s}{4\dot{\phi}^4 G_{3,X}^2} = 3 + \frac{3}{pr_1^{1+\alpha}r_2} [2p + 2q - 1 + (1 - 2p)r_1], \quad (3.48)$$

$$c_s^2 = [(2p + 2q - 1)\Omega_r - 5 + r_1(8 - 6r_1 + 3r_1^{1+\alpha}r_2) + 2p\{5 - 8r_1 + 6r_1^2 + (5 - 2q - 7r_1)r_1^{1+\alpha}r_2\} + 2q(5 - 3r_1^{2+\alpha}r_2) - 2p^2r_1^{1+\alpha}r_2(2 - 2r_1 + r_1^{1+\alpha}r_2)]/[6\{(2 - 2r_1 + r_1^{1+\alpha}r_2)p + 2q - 1 + r_1\}^2], \quad (3.49)$$

$$\mu = \Sigma = 1 + \frac{1}{\tilde{q}_s c_s^2}. \quad (3.50)$$

When $r_1 \ll 1$ and $r_2 \ll 1$, the conditions $\tilde{q}_s > 0$ and $c_s^2 > 0$ are satisfied for

$$2p + 2q - 1 > 0. \quad (3.51)$$

In this regime, expanding μ around $r_1 = 0$ and $r_2 = 0$ leads to

$$\mu = \Sigma \simeq 1 + \frac{2p}{5 + \Omega_r} r_1^{1+\alpha} r_2, \quad (3.52)$$

whose deviation from 1 is suppressed to be small.

On the tracker with $r_1 = 1$ and $r_2 \ll 1$, the stability conditions reduce to

$$\tilde{q}_s = 3 + \frac{6q}{pr_2} > 0, \quad (3.53)$$

² In the presence of quartic and quintic Horndeski interactions, this asymptotic value of w_{DE} is subject to modifications [58].

³ In Refs. [58, 66], the definition of s is half of the right hand side of Eqn. (3.47).

$$c_s^2 = \frac{6p + 10q - 3 + (2p + 2q - 1)\Omega_r}{24q^2} > 0, \quad (3.54)$$

which constrain the allowed parameter regions of p and q . Expansion of μ around $r_2 = 0$ gives

$$\mu = \Sigma \simeq 1 + \frac{4pq}{6p + 10q - 3 + (2p + 2q - 1)\Omega_r} r_2. \quad (3.55)$$

As the variable r_2 grows toward the de Sitter fixed point, the deviation of Σ from 1 tends to be larger.

At $r_1 = r_2 = 1$, the stability conditions translate to

$$\tilde{q}_s = \frac{3(p + 2q)}{p} > 0, \quad (3.56)$$

$$c_s^2 = \frac{1 - p}{3(p + 2q)} > 0. \quad (3.57)$$

For $p > 0$, we require that $p + 2q > 0$ and $p < 1$. On the de Sitter fixed point, we also have

$$\mu = \Sigma = \frac{1}{1 - p}, \quad (3.58)$$

which is larger than 1 for $0 < p < 1$.

For the data analysis, we will exploit the two parameters s and q instead of p and q . The observational constraints on the GCCG model were carried out with the data of CMB, BAO, and SNIa [66], showing that nonvanishing positive values of s are favored. The analysis with the Planck CMB data alone implies that the constrained value of H_0 is consistent with its determination from Cepheids at 1σ [65]. Moreover, it is possible to realize either positive or negative ISW-galaxy cross-correlations [66, 90], depending on the model parameters.

B. K-mouflage

We also consider K-mouflage theories in which the action in the Einstein frame is described by [67–69]

$$\mathcal{S} = \int d^4x \sqrt{-\tilde{g}} \left[\frac{M_{\text{pl}}^2}{2} \tilde{R} + \mathcal{M}^4 K(\tilde{\chi}) \right] + \mathcal{S}_{\text{m}}(\psi_{\text{m}}, g_{\mu\nu}) \quad (3.59)$$

where \mathcal{M}^4 is some energy scale, and K is a function of the dimensionless field kinetic energy given by

$$\tilde{\chi} = -\frac{\tilde{g}^{\mu\nu} \nabla_\mu \phi \nabla_\nu \phi}{2\mathcal{M}^4}. \quad (3.60)$$

We use a tilde to represent quantities in the Einstein frame. The metric $g_{\mu\nu}$ in the Jordan frame is related to $\tilde{g}_{\mu\nu}$ through a ϕ -dependent conformal factor $A(\phi)$, as

$$g_{\mu\nu} = A^2(\phi) \tilde{g}_{\mu\nu}. \quad (3.61)$$

The action \mathcal{S}_{m} depends on the matter fields ψ_{m} and the Jordan-frame metric $g_{\mu\nu}$. The matter fields in the Einstein frame (metric $\tilde{g}_{\mu\nu}$) are directly coupled to the scalar field ϕ through the conformal factor $A(\phi)$. K-mouflage theories are endowed with a screening mechanism acting in regions where the kinetic term becomes non-linear, which can suppress fifth forces induced by the coupling function $A(\phi)$. This typically happens on small cosmological scales, when the first derivative of the scalar field is large enough.

Let us consider the Jordan-frame action in the form

$$\mathcal{S} = \int d^4x \sqrt{-g} [G_4(\phi) R + G_2(\phi, X)] + \mathcal{S}_{\text{m}}(\psi_{\text{m}}, g_{\mu\nu}), \quad (3.62)$$

which corresponds to a nonminimally coupled k-essence. The Ricci scalar \tilde{R} in the Einstein frame is related to R according to $R = \tilde{R} + 6\tilde{\square}\omega - 6\tilde{g}^{\mu\nu} \partial_\mu \omega \partial_\nu \omega$, where $\omega = -\ln A$. In order to recast the action (3.62) to that in the Einstein frame under the transformation (3.61), the conformal factor $A(\phi)$ is related to $G_4(\phi)$, as

$$G_4(\phi) = \frac{M_{\text{pl}}^2}{2A^2(\phi)}. \quad (3.63)$$

Today's value of $A(\phi_0)$ is normalized to be 1 to recover the gravitational coupling $G_4(\phi_0) = M_{\text{pl}}^2/2$. Then, the Einstein-frame action following from Eqn. (3.62) is of the form

$$S = \int d^4x \sqrt{-\tilde{g}} \left(\frac{M_{\text{pl}}^2}{2} \tilde{R} + \frac{6M_{\text{pl}}^2 \mathcal{M}^4 A_{,\phi}^2}{A^2} \tilde{\chi} + A^4 G_2 \right) + \mathcal{S}_{\text{m}}(\psi_{\text{m}}, g_{\mu\nu}), \quad (3.64)$$

up to a boundary term. Here, we used the fact that the field kinetic energy $X = g^{\mu\nu} \nabla_\mu \phi \nabla_\nu \phi$ is related to $\tilde{\chi}$ as

$$\tilde{\chi} = -\frac{A^2(\phi)X}{2\mathcal{M}^4}. \quad (3.65)$$

Comparing (3.59) with (3.64), there is the following correspondence

$$G_2(\phi, X) = \frac{\mathcal{M}^4}{A^4(\phi)} K(\tilde{\chi}) - \frac{6\mathcal{M}^4 M_{\text{pl}}^2 A_{,\phi}^2(\phi)}{A^6(\phi)} \tilde{\chi}. \quad (3.66)$$

The kinetic function $K(\tilde{\chi})$ and nonminimal coupling $A(\phi)$ are the two key quantities to determine cosmic expansion and growth histories. We will study the cosmological dynamics of K-mouflage in the Jordan frame. In doing so, it is convenient to introduce the following dimensionless quantities

$$\epsilon_1 \equiv \frac{2M_{\text{pl}}^2 A_{,\phi}^2}{K_{,\tilde{\chi}} A^2}, \quad \epsilon_2 \equiv \frac{A_{,\phi} \dot{\phi}}{H A}. \quad (3.67)$$

In the Jordan frame, the Friedmann equation and scalar-field equation are given, respectively, by

$$3M_{\text{pl}}^2 H^2 (1 - \epsilon_2)^2 = A^2 (\rho_{\text{m}} + \rho_{\text{r}}) + \frac{\mathcal{M}^4}{A^2} (2\tilde{\chi} K_{,\tilde{\chi}} - K), \quad (3.68)$$

$$\frac{d}{dt} \left(A^{-2} a^3 \dot{\phi} K_{,\tilde{\chi}} \right) = -a^3 \rho_{\text{m}} \frac{A_{,\phi}}{A}. \quad (3.69)$$

The term appearing on the right hand side of Eqn. (3.69) is proportional to a trace of the matter energy-momentum tensor, so the contribution of radiation to it vanishes.

On using the general stability criteria derived for full Horndeski theories [75], the conditions for the absence of scalar ghosts and Laplacian instabilities translate, respectively, to

$$q_s = \frac{2M_{\text{pl}}^2}{A^4} (K_{,\tilde{\chi}} + 2\tilde{\chi} K_{,\tilde{\chi}\tilde{\chi}}) > 0, \quad (3.70)$$

$$c_s^2 = \frac{K_{,\tilde{\chi}}}{K_{,\tilde{\chi}} + 2\tilde{\chi} K_{,\tilde{\chi}\tilde{\chi}}} > 0, \quad (3.71)$$

which will be imposed as theoretical priors. The evolution of linear perturbations in the Jordan frame is modified by the presence of nonminimal coupling $A(\phi)$. Employing the QSA and neglecting the mass term arising from $G_{2,\phi\phi}$, the dynamics of gravitational potentials is governed by Eqs. (2.23)-(2.24), with [106]

$$\mu = (1 + \epsilon_1) A^2, \quad \Sigma = A^2, \quad (3.72)$$

so that $\mu \neq \Sigma$. The time variation of nonminimal coupling $A(\phi)$ induced by the background evolution of ϕ affects the observable associated with the ISW-galaxy cross-correlation.

To study the dark energy dynamics in K-mouflage theories, we need to specify the functional forms of $K(\tilde{\chi})$ and $A(\phi)$. In our analysis, we exploit a parameterization introduced in Ref. [69], where the time dependence of A and K is determined by five constant parameters: $\{\epsilon_{2,0}, \gamma_A, m, \alpha_U, \gamma_U\}$. The function $A(a)$ is then expressed as

$$A(a) = 1 + \alpha_A - \alpha_A \left[\frac{a(\gamma_A + 1)}{a + \gamma_A} \right]^{\nu_A}, \quad (3.73)$$

where

$$\nu_A = \frac{3(m-1)}{2m-1}, \quad \alpha_A = -\frac{\epsilon_{2,0}(\gamma_A + 1)}{\gamma_A \nu_A}, \quad (3.74)$$

where $\epsilon_{2,0}$ is today's value of ϵ_2 . The α_U and γ_U parameters contribute to the determination of $K(a)$, which can be computed by the solution of the following differential equation

$$\frac{dK}{d\tilde{\chi}} = \frac{U(a)}{a^3\sqrt{\tilde{\chi}}}, \quad (3.75)$$

with

$$U(a) = U_0 \left[\sqrt{a_{\text{eq}}} + 1 + \frac{\alpha_U}{\ln(\gamma_U + 1)} \right] \frac{a^2 \ln(\gamma_U + a)}{(\sqrt{a_{\text{eq}}} + \sqrt{a}) \ln(\gamma_U + a) + \alpha_U a^2}, \quad (3.76)$$

$$\sqrt{\tilde{\chi}} = -\frac{\rho_{\text{m},0}}{\mathcal{M}^4} \frac{\epsilon_2 A^4}{2U[(d \ln U / d \ln a) - 3\epsilon_2]}, \quad (3.77)$$

where a_{eq} is the scale factor at the epoch of matter-radiation equality, and $\rho_{\text{m},0}$ is today's value of ρ_{m} .

The theoretically allowed parameter space in K-mouflage theories were investigated in Refs. [67, 69]. For $A > 0$ and $A_{,\phi} > 0$ together with the stability conditions (3.70) and (3.71), the time derivative of ϕ being compatible with Eq. (3.69) should be in the range $\dot{\phi} < 0$. This translates to the inequality $\epsilon_2 < 0$. Taking the $\mathcal{N} = \ln a$ derivative of $\Sigma = A^2$, it follows that

$$\Sigma'(\mathcal{N}) = \epsilon_2 A^2. \quad (3.78)$$

Since $\Sigma'(\mathcal{N}) < 0$ under the condition $\epsilon_2 < 0$, the necessary condition (2.35) for realizing the negative ISW-galaxy cross-correlation is not satisfied in K-mouflage theories. This means that K-mouflage theories always give rise to a positive ISW-galaxy cross-correlation, whose property is different from those in the GGC and GCCG models.

Cosmological constraints up to linear scales using CMB, SNIa, BAO, and local measurements of H_0 set a lower 2σ limit of -0.04 for $\epsilon_{2,0}$, while the other parameters are unconstrained [106]. This is because at leading order $\epsilon_1 \simeq -\epsilon_2$ during the matter era, so most of the deviations from Λ CDM are determined by the value $\epsilon_{2,0}$. The $\epsilon_{2,0}$ parameter also impacts the ISW-galaxy cross-correlation in a two-fold way. On one hand, a higher value of $\epsilon_{2,0}$ leads to a faster cosmic expansion at late times, whose effect works to suppress the growth of matter perturbations. On the other hand, the effective dimensionless gravitational coupling $\mu = (1 + \epsilon_1)A^2$ is enhanced by the positive term ϵ_1 induced by the ϕ -dependent coupling $A(\phi)$. The trade-off between these two effects, together with the decrease of Σ in time, leads to a higher amplitude of the ISW effect in K-mouflage theories compared to its Λ CDM-limit ($\epsilon_{2,0} \rightarrow 0$).

IV. METHODOLOGY AND DATA

A. Einstein-Boltzmann code

To perform the likelihood analysis of finding the best-fit parameters of each model discussed in Sec. III, we use the publicly available Einstein-Boltzmann code `EFTCAMB` [107–109]⁴ developed to study dark energy and MG models based on the Effective Field theory (EFT) of dark energy [110, 111] (see [51, 112] for reviews). `EFTCAMB` includes `EFTCAMB_sources`, based on `CAMB_sources` [113], which is useful to extract theoretical predictions for galaxy number counts and cross-correlations with CMB. The specific models we investigate in this paper can be encoded in the EFT formalism, given the possibility to map Lagrangian-based theories with an additional scalar degree of freedom into the EFT approach [110, 111, 114–118]. In particular, we refer the reader to Ref. [64, 119] for the mapping and implementation of the GGC model, Ref. [65] for GCCG and Ref. [106] for K-mouflage. Additionally, we have implemented massive neutrinos in the EFT modules for GGC and K-mouflage. The GCCG module in `EFTCAMB` already comes with massive neutrinos.

B. The significance of the ISW

We illustrate the method for quantifying the significance of the ISW effect. To this end, we apply the likelihood code developed in Ref. [87] to MG models. After presenting the data sets to be exploited in our analysis, we illustrate

⁴ Web page: <http://www.eftcamb.org>

how we constrain the galaxy bias, which enters in Eqn. (2.22) via Eqn. (2.21). Finally, we introduce the likelihood used to provide measurements of the ISW effect through ISW-galaxy cross-correlations.

We implement cross-correlations of the CMB at large angular scales (multipoles $l \lesssim 100$) from Planck 2015 temperature data [120]⁵, with galaxy number counts from: the 2Mass Photometric Catalog (2MPZ) [121, 122], WISE x SuperCOSMOS photo- z catalog (WlXSC) [123], the Sloan Digital Sky Survey Data Release 12 (SDSS-DR12) photo- z sample [124], photometric quasars (QSO) from SDSS DR6 [125], and the National Radio Astronomy Observatory Very Large Array Sky Survey (NVSS) of extragalactic radio sources [126].

These collections of data sets provide a tracer of the large-scale structure over a redshift range $0 < z < 5$. Cross-correlations between catalogs have been removed using appropriate masks, see Ref. [87] for a detailed description. For each galaxy catalog, we use a selection function defined as a convolution of the redshift distribution of galaxies, dN/dz , and a photometric redshift error function $p(z)$. As the redshift distribution functions, we exploit the publicly available distributions obtained from Ref. [87]. For the photometric error functions, we adopt Gaussian distributions with errors defined for each catalog. For 2MPZ and QSO, we use photometric redshift errors given by $\sigma_z = 0.015$ and $\sigma_z = 0.24$, respectively. We implement redshift dependent photometric redshift errors for SDSS and WlXSC given by $\sigma_z = 0.022(1+z)$ and $\sigma_z = 0.033(1+z)$, respectively. For NVSS, we do not convolve the redshift distribution function with a photometric redshift error function as there is only one redshift bin.

In our analysis, we fix the model and cosmological parameters to the best-fit ones obtained with a combination of CMB, BAO, SNIa data as described in Sec. IV C in detail. These are then exploited to compute the expected galaxy auto-correlation \hat{C}_l^{gg} [see Eqn. (2.22)] for each catalog and redshift bin. To fit the linear bias b , we compute the χ^2 defined as

$$\chi_b^2 = \chi^2(b^2) = \sum_{l-\text{bins}} \frac{[\hat{C}_l^{\text{gg}}(b^2) - C_l^{\text{gg}}]^2}{(\Delta C_l^{\text{gg}})^2}, \quad (4.1)$$

where $\hat{C}_l^{\text{gg}}(b^2)$ assumes some value of the galaxy bias, C_l^{gg} is the measured auto-correlation power spectrum, and $(\Delta C_l^{\text{gg}})^2$ is the data covariance matrix. The sum is over all l bins. The above relation assumes that there is a unique galaxy bias factor for each redshift bin of each catalog.

At this point, along with the best-fit values for the model and cosmological parameters, we also fix the galaxy biases to their best-fit values. We then compute the ISW-galaxy cross-correlation likelihood using a χ^2 given by

$$\chi_{A_{\text{ISW}}}^2 = \chi^2(A_{\text{ISW}}) = \sum_{\text{catg.}} \sum_{z-\text{bins}} \sum_{l-\text{bins}} \frac{(A_{\text{ISW}} \hat{C}_l^{\text{Tg}} - C_l^{\text{Tg}})^2}{(\Delta C_l^{\text{Tg}})^2}, \quad (4.2)$$

where \hat{C}_l^{Tg} is the measured cross-correlation power spectrum, \hat{C}_l^{Tg} is the theory cross-correlation power spectrum obtained with the best-fit parameters, and $(\Delta C_l^{\text{Tg}})^2$ is the data covariance matrix. The only free parameter in the above relation is the amplitude A_{ISW} . This is then the parameter for which we fit to data. A_{ISW} is assumed to take on a fiducial value of 1. When $A_{\text{ISW}} \neq 1$, it rescales the amplitude of the theoretical ISW-galaxy cross-correlation power spectrum. In detail, $A_{\text{ISW}} > 1$ corresponds to the theory predicting a lower ISW power relative to the measured one, while the opposite holds for $A_{\text{ISW}} < 1$.

We compute the mean and standard deviation for A_{ISW} and the galaxy bias parameters using the following method. For a general parameter B that rescales a theory vector \mathbf{t} relative to some data vector \mathbf{d} and some data covariance matrix \mathbb{C} , the best-fit value can be analytically derived by minimizing the χ^2 with respect to B finding

$$B_{\text{bf}} = \frac{\mathbf{d}^T \mathbb{C}^{-1} \mathbf{t}}{\mathbf{t}^T \mathbb{C}^{-1} \mathbf{t}}, \quad (4.3)$$

with variance given by

$$\sigma_B^2 = \frac{1}{\mathbf{d}^T \mathbb{C}^{-1} \mathbf{t}}. \quad (4.4)$$

Assuming that the amplitude parameter distribution is approximately Gaussian, the mean value of B is approximately equivalent to the best-fit value of B . Since both A_{ISW} and the galaxy bias parameters rescale the amplitude of the cross- and auto-correlation power spectra, respectively, it follows that this analytic formulation can be applied to their cases.

⁵ Planck 2018 temperature data are more up to date, but the differences between 2015 and 2018 releases were primarily found in improvements to polarization. Hence it is unlikely that the differences between two data sets for $l \lesssim 100$ lead to a significant change [16].

We created a code implementing the methodology described above. We aim to make it public in the near future. To test the robustness of our implementation, we compared our results for the galaxy bias and A_{ISW} parameters with the ones in Ref. [87] assuming the Λ CDM model for which the best-fit cosmological parameters are fixed to the Planck 2015 results. We found that the galaxy bias factors are consistent with the values in Ref. [87]. Furthermore, we confirmed that adopting either the values reported in Ref. [87] or those computed with our code results in a negligible change for A_{ISW} . To be concrete, we obtained the constraint $A_{\text{ISW}} = 1.54 \pm 0.32$, which is within 0.1σ of $A_{\text{ISW}} = 1.51 \pm 0.30$ as reported in Ref. [87]. Hence the codes used to compute these quantities are in agreement with each other.

Before concluding this subsection, we would like to stress that, instead of using the best-fit values in the analysis, one can alternatively resort to a full Markov Chain Monte Carlo (MCMC) approach that varies all of the parameters along with the galaxy bias factors and A_{ISW} . In the Λ CDM model, it has been found that both methods give the same conclusion [87]. In this work, we then adopt the best-fit approach for simplicity. We will leave a full MCMC analysis for a future work.

C. Best-fit values for cosmological and model parameters

For the purpose of the present work, it is sufficient to exploit only the best-fit values for the cosmologies we are interested in. They are obtained from minimization instead of full Markov Chain Monte Carlo (MCMC), as mentioned in the previous subsection. For this purpose, we run EFTCosmoMC [108] and combine the following data sets:

- *Planck* 2018 measurements of CMB temperature and polarization anisotropy [127]. In detail, we use the TT and EE power spectra, and TE cross-correlations over small angular scales ($\ell \in [30, 2508]$ for TT power spectrum, $\ell \in [30, 1996]$ for TE cross-correlation and EE power spectra). In all cases, we use the Pliklite likelihood, which marginalizes over foreground parameters.
- Measurements of the BAO from BOSS DR12 [128], SDSS Main Galaxy Sample DR7 [129], and 6dFGS [130].
- The 2018 Pantheon Supernova compilation [11], which includes 1048 SNIa data in the redshift range $0.01 < z < 2.3$.

Hereafter, we refer to this combination of data as Baseline. Let us note that we do not include CMB lensing data by *Planck* because of the dependence of the lensing potential power spectrum at multipole $\ell > 100$ on the parameters of the Λ CDM model [131]. For each minimization, we use the best-fit parameters found by an MCMC as a starting point for the minimization code. We use the built-in EFTCosmoMC minimization code. The best-fit parameters for the Λ CDM, GGC, GCCG, and K-mouflage models are presented in Table I. In this table, $H_0 = 100 h \text{ km sec}^{-1} \text{ Mpc}^{-1}$ is today's Hubble parameter, $\Omega_{b,0}$ and $\Omega_{c,0}$ are today's density parameters of baryons and CDM respectively, A_s and n_s are the amplitude and scalar spectral index of primordial curvature perturbations, τ is the optical depth, and $S_8 = \sigma_{8,0} \sqrt{\Omega_{m,0}/0.3}$, where $\sigma_{8,0}$ is today's amplitude of matter perturbations at the scale $8h^{-1} \text{ Mpc}$.

For the K-mouflage minimization, we fixed three out of five model parameters to $m = 3$, $\gamma_A = 0.2$, and $\gamma_U = 1$ as they are unconstrained by cosmological observables [106]. We have also included the Λ CDM best-fit values of cosmological parameters for reference. In all cases, we include massive neutrinos with fixed total mass of $\sum m_\nu = 0.06 \text{ eV}$.

Each MG model fits this combination of likelihoods slightly better than Λ CDM as seen by the χ^2 comparison in Table II. For the GGC and GCCG models, the reduction in χ^2 with respect to Λ CDM is $\Delta\chi^2 = -7.6$ and $\Delta\chi^2 = -5.1$, respectively. This comes primarily from a better fit to *Planck* CMB anisotropy data as shown in Table II where it is clear that the actual improvement comes from the TTTEEE data for $\ell > 30$. This result has been previously discussed in Refs. [64, 65]. Since the inclusion of additional parameters might lead to a better fit to the data, only a proper model selection analysis based not only on the goodness of fit but also on the complexity of the model can actually inform if the model is preferred by data or not. This kind of analysis is out of the scope of the present work. However, a similar investigation has been performed for these two models when a proper MCMC analysis is adopted, and it has been found that for some combinations of data they are preferred over Λ CDM [64, 65].

The best-fit K-mouflage model gives only a slight difference $\Delta\chi^2 = -0.3$ relative to Λ CDM, so it is essentially degenerate to the Λ CDM limit. Therefore, it is unlikely that the combination of data sets used in our analysis will prefer K-mouflage over Λ CDM even by varying all five parameters.

V. RESULTS AND DISCUSSION

We now confront theoretical predictions of the GGC, GCCG, and K-mouflage models with the measurements of ISW-galaxy cross-correlations. For the purpose of understanding how the presence of additional model parameters

Model	H_0	$\Omega_{b,0}h^2$	$\Omega_{c,0}h^2$	$10^9 A_s$	n_s	τ	S_8	Additional model parameters	χ^2
Λ CDM	67.69	0.02242	0.1193	2.099	0.9673	0.055	0.8234	–	2044.8
GGC	68.24	0.02245	0.1196	2.108	0.9656	0.057	0.8502	$x_1^0 = -1.20, x_3^0 = 0.38$	2037.2
GCCG	68.93	0.02240	0.1200	2.106	0.9656	0.056	0.8394	$s = 0.182, q = 1.49$	2039.7
K-mouflage	68.37	0.02241	0.1198	2.106	0.9670	0.056	0.8250	$\alpha_U = 0.505, \epsilon_{2,0} = -6.9 \times 10^{-4}$	2044.5

Table I. Best-fit cosmological parameters and corresponding χ^2 values derived from likelihood minimization fits of the Λ CDM, GGC, GCCG, and K-mouflage models, respectively (see Sec. III). For the K-mouflage case, we fix $\gamma_U = 1, \gamma_A = 0.2, m = 3$ as these parameters are unconstrained by the likelihood.

Model	<i>Planck</i> 2018 TTTEEE $\ell > 30$	<i>Planck</i> TT $\ell \leq 30$	<i>Planck</i> LowE	SN	BAO	χ^2	$\Delta\chi^2$
Λ CDM	584.9	23.0	396.1	1035.0	5.7	2044.8	0
GGC	578.0	22.3	396.6	1034.7	5.5	2037.2	-7.6
GCCG	580.0	22.2	396.4	1035.0	6.132	2039.7	-5.1
K-mouflage	584.7	23.2	396.4	1034.8	5.4	2044.5	-0.3

Table II. Breakdown in the χ^2 by likelihood used for the best-fit Λ CDM, GGC, GCCG, and K-mouflage models, respectively (see Sec. III). In the Table we define $\Delta\chi^2 = \chi_{\text{MG}}^2 - \chi_{\Lambda\text{CDM}}^2$ at the difference between MG and Λ CDM in the total χ^2 .

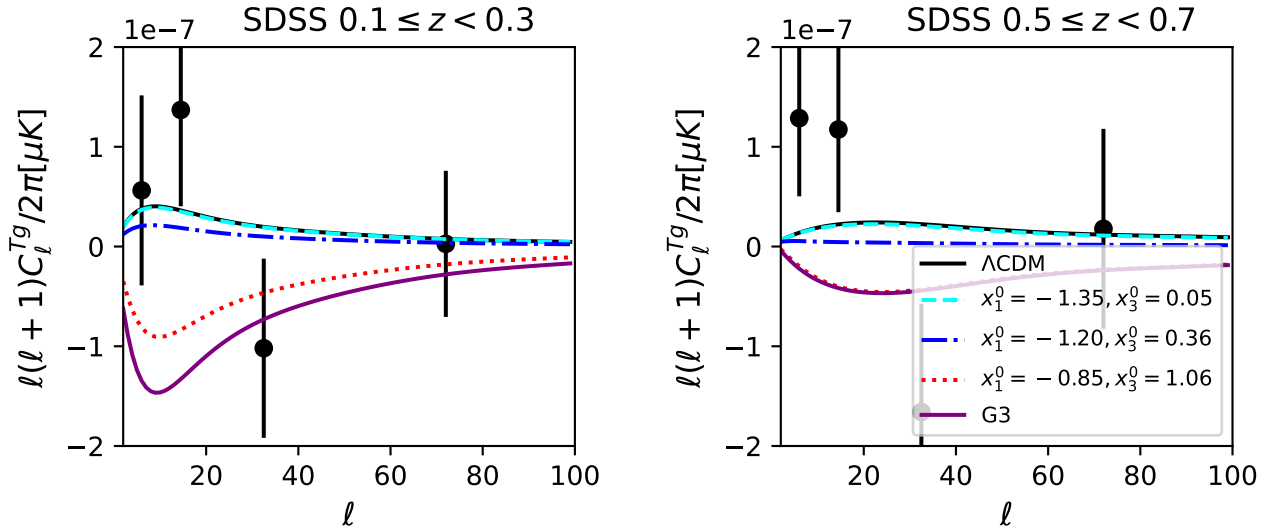


Figure 1. In the GGC model, we plot the ISW-galaxy cross-correlation power spectra for two different redshift bins: (1) $0.1 \leq z < 0.3$ (left) and (2) $0.5 \leq z < 0.7$ (right). We show $l(l+1)C_l^{Tg}/(2\pi)$ for three different cases: (i) $x_1^0 = -1.35, x_3^0 = 0.05$, (ii) $x_1^0 = -1.20, x_3^0 = 0.36$, and (iii) $x_1^0 = -0.85, x_3^0 = 1.06$, where x_1^0 and x_3^0 are today's values of x_1 and x_3 respectively. The SDSS data are shown as black points with error bars. Besides the Λ CDM model, we also depict the cross-correlation power spectrum in the Cubic Galileon (G3) model. In all cases, we fix the Λ CDM model parameters to the Λ CDM best-fit values presented in Table I. If the magnitude of $|x_1^0|$ increases relative to x_3^0 , the ISW signal approaches the Λ CDM limit. For x_3^0 exceeding the order of $|x_1^0|$, the ISW signal approaches the G3 limit. In this latter case, it is possible to generate a negative ISW-galaxy cross-correlation, which is disfavored when data from all redshift bins are included.

to those in the Λ CDM model modifies the ISW-galaxy cross-correlation power spectra, we first show the theoretical values of $l(l+1)C_l^{Tg}/(2\pi)$ for the same best-fit cosmological parameters as those in Λ CDM. Then, using the best-fit parameters derived using the Baseline likelihood for each model, we study whether the three classes of MG models can be compatible with the ISW-galaxy cross-correlation data. In the following, we will discuss each model in turn.

Catalog	z	Λ CDM	GGC	GCCG	K-mouflage
SDSS	0.1-0.3	1.16	1.12	1.12	1.15
	0.3-0.4	1.04	1.00	1.01	1.03
	0.4-0.5	1.01	0.98	0.99	1.00
	0.5-0.7	1.40	1.36	1.37	1.38
	0.7-1.0	1.41	1.39	1.40	1.41
WISS	0.09-0.21	1.12	1.08	1.09	1.11
	0.21-0.3	1.00	0.97	0.98	0.99
	0.3-0.6	1.30	1.26	1.26	1.29
QSO	0.5-1	2.22	2.17	2.19	2.20
	1-2	3.09	3.00	3.02	3.02
	2-3	3.88	3.85	3.87	3.86
2MPZ	0-0.105	1.24	1.19	1.20	1.23
	0.105-0.195	1.43	1.38	1.39	1.42
	0.195-0.3	2.13	2.06	2.07	2.11
NVSS	0-5	2.22	2.15	2.16	2.20

Table III. Best-fit galaxy bias factors b for each redshift bin of five different catalogs. We consider four different cosmological models with fiducial parameters given in Table I.

A. Galileon Ghost Condensate (GGC)

In the GGC model, the existence of the Galileon Lagrangian $3a_3 X \square \phi$ gives rise to a different cosmic growth history compared to Λ CDM. As we observe in Eq. (3.34), the variable x_3 leads to deviations of μ and Σ from 1. In Fig. 1, we plot the ISW-galaxy cross-correlation power spectrum for several different sets of the GGC model parameters x_1^0 and x_3^0 (which are today's values of x_1 and x_3). In the same figure, we also include the Λ CDM and G3 models for comparison. To plot the power spectra for each model in Fig. 1, we fix the Λ CDM model parameters for each of the models depicted to the Λ CDM best-fit values presented in Table I.

In Fig. 1, we also show data from the cross-correlation of SDSS galaxy number counts with *Planck* temperature data in the redshift ranges $0.1 \leq z < 0.3$ and $0.5 \leq z < 0.7$. For the theoretical power spectra, we adopt the same selection function as used in the two redshift ranges of SDSS to elucidate the power spectrum for those particular redshift bins. Overall, the strength of ISW signal is weaker in the higher redshift bin than in the lower redshift bin as the scalar field is subdominant to the background fluid at earlier times.

As we observe in Fig. 1, irrespective of the redshift bins, larger values of x_3^0 work to suppress the ISW-galaxy cross-correlation power with respect to Λ CDM. In the limit $x_3^0 \rightarrow 0$, GGC mimics Λ CDM. As x_3^0 exceeds the order of $|x_1^0|$, GGC approaches the G3 limit. In Fig. 2, we plot the evolution of \mathcal{F} defined by Eqn. (2.29) for the same model parameters as those used in Fig. 1. From Eqn. (2.30), the negative ISW-galaxy cross-correlation is accompanied by negative values of \mathcal{F} , whose property can be confirmed by comparing Fig. 1 with Fig. 2. For increasing ratio $x_3^0/|x_1^0|$, \mathcal{F} becomes negative in most of the low redshift ranges. This leads to the suppressed ISW-galaxy cross-correlation power $l(l+1)C_l^{\text{Tg}}/(2\pi)$, whose behavior is not favored from the SDSS data shown in Fig. 1.

For the best-fit parameters presented in Table I, we compute the auto-correlation χ^2 given by Eqn. (4.1). Then, we find the best-fit galaxy bias parameters, which are given in Table III. The obtained values of b in GGC are similar to those in Λ CDM. Using the best-fit parameters along with these galaxy bias values, we calculate the χ^2 in Eqn. (4.2) for the ISW-galaxy cross-correlation power spectra. We consider the two cases: (1) A_{ISW} is fixed to 1, and (2) A_{ISW} is allowed to vary. The χ^2 values for cases (1) and (2) are denoted as χ_1^2 and χ_A^2 , respectively. The constrained values of χ_1^2 and χ_A^2 are presented in Table IV. In Λ CDM the value of A_{ISW} derived by the ISW likelihood is slightly different from the one reported in Sec. IV B, because here we are using different fiducial Λ CDM parameters.

We find that the GGC best-fit model has a worse fit to the likelihood than Λ CDM as quantified by an increase in both χ_1^2 and χ_A^2 . This increase of χ^2 in GGC results from the reduction of power in the ISW signal. The suppressed ISW power manifests itself in the preference for larger $A_{\text{ISW}} = 2.71 \pm 0.94$ in comparison to the Λ CDM bound $A_{\text{ISW}} = 1.61 \pm 0.33$. The increases $\Delta\chi_1^2 = 15.7$ and $\Delta\chi_A^2 = 15.3$ for the GGC best-fit relative to the Λ CDM best-fit are greater than the reduction $\Delta\chi^2 = -7.6$ for the GGC best-fit relative to the Λ CDM best-fit for the fit to the Baseline likelihood. This means that the GGC best-fit parameters shown in Table I are not compatible with the ISW likelihood when combined with the Baseline data.

In Tables V and VI, we show the contributions to the χ^2 arising from each redshift bin of the catalogs we are using. The largest contributions in both χ_1^2 and χ_A^2 come from the higher redshift bins with NVSS alone, contributing $\Delta\chi_1^2 = 5.92$ and $\Delta\chi_A^2 = 6.66$, respectively. There are also increases of $\Delta\chi_1^2 > 1$ and $\Delta\chi_A^2 > 1$ resulting from SDSS in the ranges $0.4 \leq z < 0.5$ and $0.5 \leq z < 0.7$ as well as QSO in the ranges $0.5 \leq z < 1$ and $1 \leq z < 2$. Excluding any

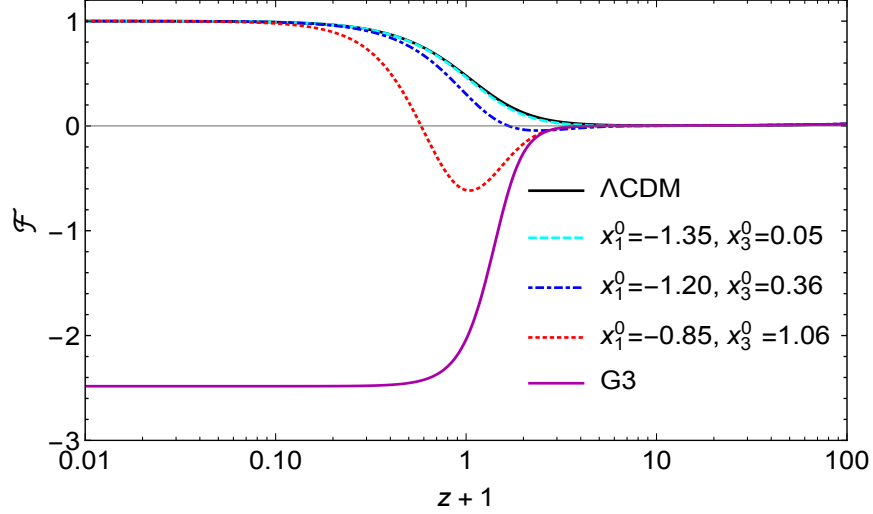


Figure 2. Evolution of the quantity \mathcal{F} versus $z+1$ for three different cases of the GGC model: (i) $x_1^0 = -1.35$, $x_3^0 = 0.05$, (ii) $x_1^0 = -1.20$, $x_3^0 = 0.36$, and (iii) $x_1^0 = -0.85$, $x_3^0 = 1.06$. We include the plots of Λ CDM and G3 models as reference. As the ratio $x_3^0/|x_1^0|$ increases, \mathcal{F} becomes negative in most of the low redshift range. A negative value of \mathcal{F} is a necessary, though not sufficient condition, for a negative ISW-galaxy cross-correlation.

Model	A_{ISW}	χ_1^2	A_{ISW}	χ_A^2
Λ CDM	1	47.1	1.61 ± 0.33	43.4
GGC	1	62.8	2.71 ± 0.94	58.7
GCCG	1	58.6	4.22 ± 0.90	44.9
K-mouflage	1	46.9	1.59 ± 0.33	43.4

Table IV. For four different cosmological models, we show χ_1^2 for $A_{\text{ISW}} = 1$ and χ_A^2 when A_{ISW} is allowed to vary. They are derived by using best-fit cosmological parameters extracted from the likelihood minimization (see Sec. IV C).

one of the entire catalogs would result in increases of χ_1^2 and χ_A^2 . This increase is sufficient to offset the reduction of χ^2 shown in Table II. Therefore, the fact that the GGC best-fit model is incompatible with the ISW likelihood in comparison to the Λ CDM best-fit model is not associated with a systematic error in one of the data sets or redshift bins. Additionally, even when the phenomenological rescaling of A_{ISW} is used, the χ^2 in GGC is significantly larger than that in Λ CDM. This suggests that the worse fit relative to Λ CDM is not only the result of a reduction of the ISW power, but also of a change in the shape of the power spectrum. In particular we find that, for high redshift measurements of QSO and NVSS, the best-fit GGC model has a negative ISW-galaxy cross-correlation.

B. Generalized Cubic Covariant Galileon (GCCG)

As we discussed in Sec. III A 2, the key quantities of the GCCG model affecting the cosmic expansion and growth histories are the two parameters q and $s = p/q$. At the background level, the deviation of w_{DE} from -1 is quantified by the parameter s . For the tracker solution, the deviations of μ and Σ from 1 are proportional to $4sq^2r_2$, see Eqn. (3.55). This means that, for increasing values of s or q , the evolution of perturbations is generally subject to modifications in comparison to Λ CDM.

In Fig. 3, we depict the ISW-galaxy cross-correlation power spectra for the GCCG model for several different values of s and q . We also include the plots for the Λ CDM and G3 models, together with data from the SDSS catalog. For the theory power spectra, we use the same selection function as used by the SDSS redshift bins. In this figure, we choose cosmological parameters present in both Λ CDM and MG models to be the Λ CDM best-fit values given in Table I. Depending on the values of s and q , it is possible to realize both positive and negative cross-correlations. As we see in Fig. 3, increasing the values of either s or q works to suppress the ISW-galaxy cross-correlation power relative to Λ CDM. In particular, the cross-correlation becomes negative for large products sq .

As in the GGC model, we evaluate the best-fit values of bias factors b according to Eqn. (4.1) by adopting the best-

Catalog	z	$\chi^2_{1,\Lambda\text{CDM}}$	$\Delta\chi^2_{1,\text{GGC}}$	$\Delta\chi^2_{1,\text{GCCG}}$	$\Delta\chi^2_{1,\text{KM}}$
SDSS	0.1-0.3	2.85	0.08	0.13	0.00
	0.3-0.4	1.59	0.85	0.80	-0.01
	0.4-0.5	2.50	1.64	1.42	-0.02
	0.5-0.7	5.95	2.51	1.98	-0.04
	0.7-1.0	6.42	0.09	0.16	0.00
WISS	0.09-0.21	2.34	-0.18	-0.20	0.01
	0.21-0.3	3.10	0.41	0.49	-0.01
	0.3-0.6	1.98	0.06	0.05	0.00
QSO	0.5-1	5.38	1.72	1.17	-0.02
	1-2	1.31	1.80	0.78	-0.01
	2-3	3.67	0.46	0.16	0.00
2MPZ	0-0.105	2.04	0.05	0.07	0.00
	0.105-0.195	0.67	0.05	0.09	0.00
	0.195-0.3	0.69	0.24	0.29	0.00
NVSS	0-5	6.56	5.92	4.14	-0.06

Table V. The differences of χ^2_1 between three MG models and ΛCDM , i.e., $\Delta\chi^2_{1,x} = \chi^2_{1,x} - \chi^2_{1,\Lambda\text{CDM}}$, where x denotes either GGC, GCCG, K-mouflage (KM) models. The χ^2_1 values in ΛCDM are also presented. In all cases, $A_{\text{ISW}} = 1$. We show the values of $\Delta\chi^2_{1,x}$ for each redshift bin of five different catalogs of the ISW-galaxy cross-correlation likelihood.

Catalog	z	$\chi^2_{A,\Lambda\text{CDM}}$	$\Delta\chi^2_{A,\text{GGC}}$	$\Delta\chi^2_{A,\text{GCCG}}$	$\Delta\chi^2_{A,\text{KM}}$
SDSS	0.1-0.3	3.22	-0.28	0.09	0.00
	0.3-0.4	1.33	0.39	0.02	0.00
	0.4-0.5	1.72	1.36	0.18	0.00
	0.5-0.7	4.86	2.54	0.32	-0.01
	0.7-1.0	6.41	-0.38	-0.25	0.00
WISS	0.09-0.21	2.78	-0.13	0.20	0.00
	0.21-0.3	3.10	-0.14	-0.04	0.00
	0.3-0.6	2.34	-0.35	-0.07	0.00
QSO	0.5-1	4.86	1.90	0.10	0.00
	1-2	1.05	3.00	-0.06	0.00
	2-3	3.59	0.89	0.05	0.00
2MPZ	0-0.105	1.99	-0.01	-0.01	0.00
	0.105-0.195	0.76	-0.02	0.09	0.00
	0.195-0.3	0.75	-0.06	0.05	0.00
NVSS	0-5	4.62	6.66	0.88	0.00

Table VI. The differences of χ^2_A between three MG models and ΛCDM , i.e., $\Delta\chi^2_{A,x} = \chi^2_{A,x} - \chi^2_{A,\Lambda\text{CDM}}$, where x denotes either GGC, GCCG, K-mouflage (KM) models. The χ^2_A values in ΛCDM are also shown. In all cases, A_{ISW} 's are fixed to the best-fit values shown in Table IV. We present the values of $\Delta\chi^2_{A,x}$ for each redshift bin of five different catalogs of the ISW-galaxy cross-correlation likelihood.

fit model and cosmological parameters given in Table I. The best-fit values of b in the GCCG, which are presented in Table III, are similar to those in the ΛCDM case. We also compute the χ^2 of the ISW-galaxy cross-correlation power spectra given by Eqn. (4.2). In Table IV we show the values of χ^2_1 and χ^2_A , which are derived by setting $A_{\text{ISW}} = 1$ and by varying A_{ISW} respectively. The χ^2 for the Baseline likelihood alone exhibits a better fit to data relative to ΛCDM ($\Delta\chi^2 = -5.1$). Taking into account the ISW-galaxy cross-correlation data; however, the χ^2_1 in GCCG is larger than the ΛCDM value, with difference $\Delta\chi^2_1 = 11.5$. This suggests that GCCG best-fit model given in Table I is not compatible with the ISW-galaxy likelihood when combined with the Baseline data.

Allowing A_{ISW} to vary, we find that the difference of $\Delta\chi^2_A$ between the best-fit GCCG and the best-fit ΛCDM models is $\Delta\chi^2_A = 1.5$, which is smaller than $\Delta\chi^2_1 = 11.5$ obtained for $A_{\text{ISW}} = 1$. The constraint on A_{ISW} is $A_{\text{ISW}} = 4.22 \pm 0.90$, so the best-fit GCCG model predicts a smaller ISW power compared to the ΛCDM model. Since the difference $\Delta\chi^2_A$ between the best-fit GCCG and best-fit ΛCDM models is closer to zero when A_{ISW} is allowed to vary, it follows that the suppression of ISW power for the best-fit GCCG is the primary reason for the incompatibility with the ISW-galaxy data relative to ΛCDM .

In Tables V and VI, we show the relative differences of χ^2_1 as well as χ^2_A between three MG models and ΛCDM for each redshift bin of the five catalogs. As in the best-fit GGC model, the preference for larger values of χ^2_1 in the best-fit GCCG arises from the high redshift bins with NVSS alone contributing $\Delta\chi^2_1 = 4.14$. There are also increases in $\Delta\chi^2_1 > 1$ resulting from SDSS in the ranges $0.4 \leq z < 0.5$ and $0.5 \leq z < 0.7$ as well as QSO in the region

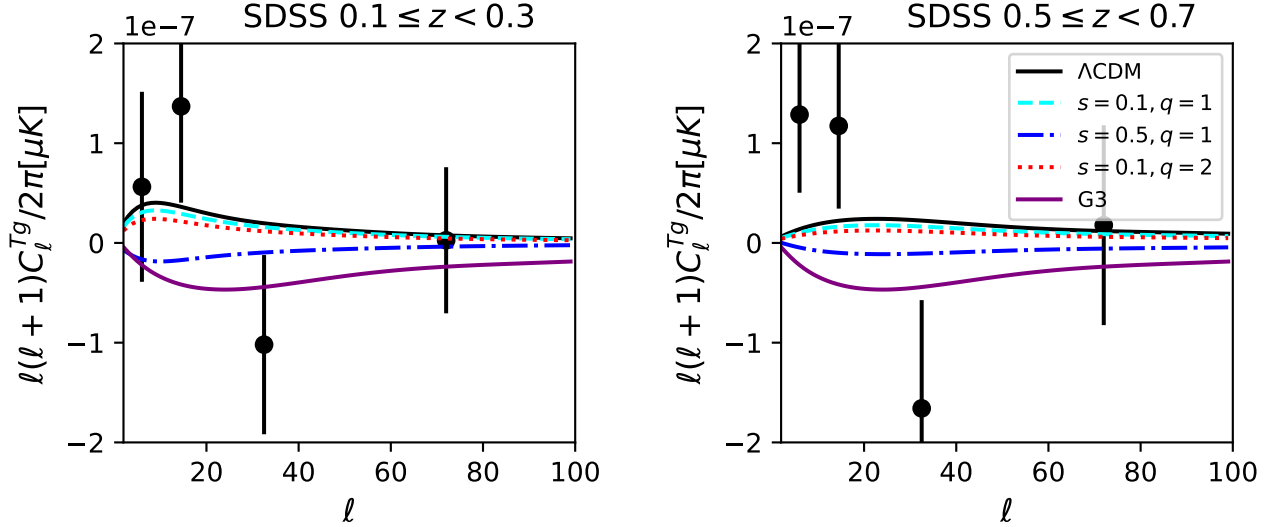


Figure 3. The ISW-galaxy cross-correlation power spectra for the GCCG model for two redshift bins. The data points are the same as those in Fig. 1. Each case corresponds to the model parameters (i) $s = 0.1$, $q = 1$, (ii) $s = 0.5$, $q = 1$, and (iii) $s = 0.1$, $q = 2$. We also plot the cross-correlation power spectra in Λ CDM and G3 models. In all cases, we fix the parameters present in the Λ CDM model to the Λ CDM best-fit values given in Table I. For increasing values of s or q the evolution of perturbations exhibits a larger deviation from that in Λ CDM, in which case it is possible to generate negative ISW-galaxy cross-correlations. This negative cross-correlation is disfavored when data from all redshift bins are included.

$0.5 \leq z < 1$. Removing any one of the entire photometric galaxy catalogs still results in an increase of χ^2_1 greater than the improvement of the best-fit GCCG in the χ^2 fit to the Baseline likelihood relative to the best-fit Λ CDM case. This suggests that the incompatibility of GCCG best-fit to the ISW-galaxy cross-correlation likelihood relative to Λ CDM best-fit is not attributed to a systematic error in any one of the data sets or redshift bins.

C. K-mouflage

As we discussed in Sec. III B, a key quantity that determines the cosmic expansion and growth histories in the K-mouflage model is the parameter $\epsilon_{2,0}$. In Fig. 4 we show the theoretical predictions of the ISW-galaxy cross-correlation power spectra for several choices of $\epsilon_{2,0}$, together with the SDSS data in two different redshift bins. We fix parameters present in the Λ CDM model, to the Λ CDM best-fit values in Table I. We use the same selection function for the theory power as used by the SDSS data in the specific redshift bin. We observe that larger negative values of $\epsilon_{2,0}$ result in an increase of the ISW-galaxy cross-correlation power spectra compared to those in Λ CDM (which corresponds to the limit $\epsilon_{2,0} \rightarrow 0$). This is associated with the fact that the quantity Σ decreases in time for $\epsilon_2 < 0$, so the ISW-galaxy cross-correlation is always positive. Moreover, the quantities $\mu = (1 + \epsilon_1)A^2$ and $\Sigma = A^2$ are larger than 1 in the past for the normalization $A(\phi_0) = 1$ today. Since the variation of $A(\phi)$ occurs mostly at late times, the deviations of $l(l+1)C_l^{Tg}/(2\pi)$ from the Λ CDM case in the redshift range $0.1 \leq z < 0.3$ are more significant than those in the range $0.5 \leq z < 0.7$.

The maximum likelihood Baseline likelihood analysis shows that the best-fit value of $\epsilon_{2,0}$ is -6.9×10^{-4} (see Table I), which is relatively close to zero. Hence only minimal deviations from the Λ CDM model are allowed from joint constraints with the CMB, BAO, and SNIa data for both the background and perturbations. This phenomenology improves the fit to the ISW cross-correlation between CMB temperature anisotropy and galaxy number counts. For $A_{\text{ISW}} = 1$, as shown in Table IV, the χ^2 value is improved only by $\Delta\chi^2_1 = -0.2$ compared to Λ CDM. If A_{ISW} is allowed to vary, the χ^2_A values for K-mouflage and Λ CDM are exactly the same for their best-fit parameters. This suggests that the only difference between the two model predictions comes from a slight preference for more ISW power in the K-mouflage case. In terms of A_{ISW} the K-mouflage model predicts $A_{\text{ISW}} = 1.59 \pm 0.33$, while the Λ CDM value $A_{\text{ISW}} = 1.61 \pm 0.33$ is slightly larger.

In the future, we plan to use more updated catalogs such as the DESI data [95], especially in light of the minor differences in the measured values of A_{ISW} between DESI and our collection of catalogs for the Λ CDM scenario. Indeed, according to the results we obtained for the Λ CDM model with the Planck 2018 best-fit values, we find

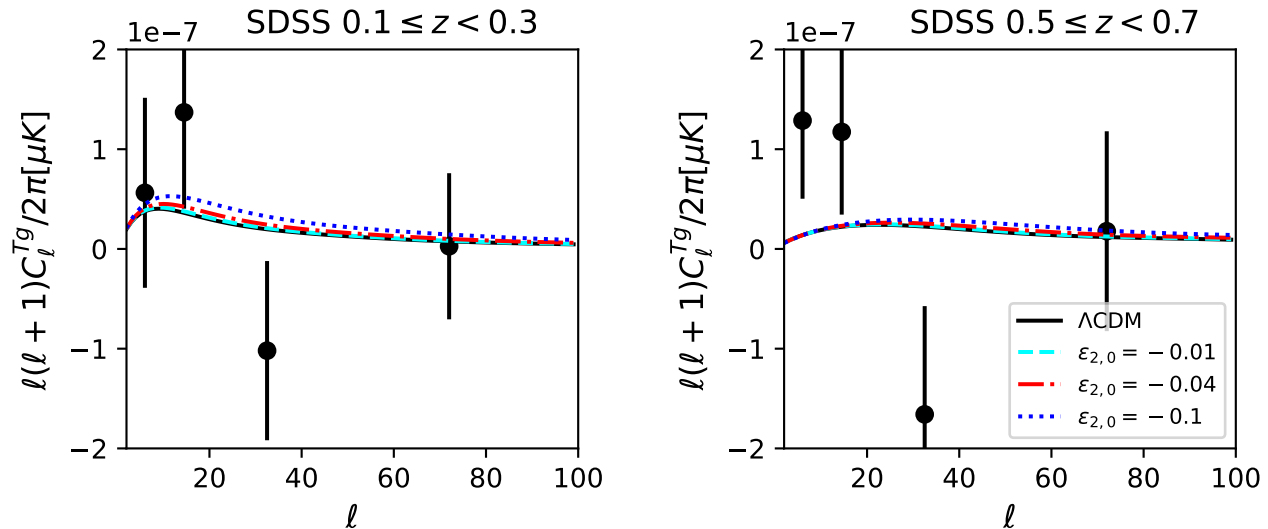


Figure 4. The ISW-galaxy cross-correlation power spectra for two redshift bins in the K-mouflage model. The data points are the same as those in Fig. 1. Each case corresponds to the model parameters (i) $\epsilon_{2,0} = -0.01$, (ii) $\epsilon_{2,0} = -0.04$, and (iii) $\epsilon_{2,0} = -0.1$, together with the plot of the Λ CDM model (which corresponds to the limit $\epsilon_{2,0} \rightarrow 0$). In all cases, the parameters present in Λ CDM are fixed to the Λ CDM best-fit values shown in Table I. For decreasing $|\epsilon_{2,0}|$, the ISW-galaxy cross-correlation power spectra are subject to the mild enhancement in comparison to those in Λ CDM. At higher redshifts, the differences between K-mouflage and Λ CDM models tend to be smaller.

$A_{\text{ISW}} > 1$ at 1.85σ . This implies that Λ CDM is predicting less power for the ISW-galaxy cross-correlation power spectrum than is being measured. In Ref. [95], this preference for $A_{\text{ISW}} > 1$ is not found in the cross-correlation between the DESI Legacy Survey and Planck 2018 data. Constraints from DESI would be an interesting test for MG models.

VI. CONCLUSION

In this paper, we studied the ISW-galaxy cross-correlation to probe three MG models of dark energy, i.e., GGC, GCCG, and K-mouflage models. For this purpose, we have used a tomographic analysis of the ISW signal based on photometric measurements of the redshift of galaxies following the prescription in Ref. [87]. The previous analysis assumed the standard flat Λ CDM cosmological model, so we extended it to include MG models in the framework of Horndeski theories. The GGC and GCCG models contain the cubic-order derivative interaction $G_3(X)\Box\phi$, which can induce negative ISW-galaxy cross-correlations. On the other hand, the K-mouflage model gives rise to only the positive cross-correlation. These properties can be used to distinguish between different MG models from the ISW-galaxy cross-correlation power spectrum.

In our analysis, we first found the best-fit parameters for each of the cosmological models derived by joint constraints with the CMB, BAO and SNIa data. They are given in Table I for the GGC, GCCG, and K-mouflage models besides Λ CDM. Then, these best-fit parameters were used as a fiducial model to compute the χ^2 values in a fit to the ISW-galaxy cross-correlation and the collection of photometric redshift survey. This analysis was performed for two cases; one where we included a phenomenological rescaling of the theoretical cross-correlation curve via a parameter A_{ISW} , and the other where A_{ISW} is fixed to one. In the case where A_{ISW} is allowed to vary, we summarize the best-fit values of A_{ISW} for each model in Table IV.

When A_{ISW} is kept fixed to 1, the GGC and GCCG best-fit models are incompatible with the ISW-galaxy cross-correlation data relative to the Λ CDM best-fit model. This is mostly attributed to the fact that the best-fit values for the GGC and GCCG models prefer a suppressed ISW signal compared to Λ CDM, which reduces the power in the ISW-galaxy cross-correlation. As we observe in Figs. 1 and 3, these models can give rise to negative ISW-galaxy cross-correlations when the quantity Σ grows rapidly to reach the regime $\mathcal{F} < 0$. Indeed, this increase of Σ induced by the cubic coupling $G_3(X)\Box\phi$ leads to the suppressed ISW-galaxy cross-correlation power spectrum in comparison to Λ CDM, whose property tends to be incompatible with the observational data.

For the GCCG best-fit model, the suppressed ISW signal can be offset by a larger value of A_{ISW} than in Λ CDM.

For the GGC best-fit model, allowing A_{ISW} to vary for the best-fit parameters derived by Baseline likelihood is not sufficient to bring it into comparable agreement with the ISW-galaxy cross-correlation data as the Λ CDM best-fit case. These results show that, while the suppression of ISW power in GCCG is the main reason for the tension with data, the modification of ISW-galaxy cross-correlation power spectrum itself in GGC largely contributes to the incompatibility with data. The K-mouflage model has best-fit parameters whose deviations from Λ CDM are small, in addition to the fact that the ISW power is always positively correlated with galaxy fluctuations. We find that K-mouflage cannot be distinguished from Λ CDM even by adding the ISW-galaxy cross-correlation data.

In the future, we plan to perform a further exploration with a proper MCMC analysis to constrain the whole parameter space. This will allow us to perform a model selection analysis and see whether the GCG and GCCG models are ruled out or not by ISW-galaxy cross-correlation data. Furthermore, as more and more photometric measurements of redshift of galaxies are gathered, the errors from the ISW-galaxy cross-correlation will be reduced. With such future high-precision measurements, it will be possible to scrutinize the possible large-distance modifications of gravity.

ACKNOWLEDGMENTS

JK and GB wish to thank Charles Bennett, Graeme Addison, and Janet Weiland for many stimulating discussions during the analysis and write up for this work. Additionally, we wish to thank Simone Peirone for collaboration in the early stages of the work. For JK and GB, this work was performed, in part, for the Jet Propulsion Laboratory, California Institute of Technology, sponsored by the United States Government under the Prime Contract 80NM00018D0004 between Caltech and NASA under subcontract numbers 1643587 and 1658514. This research project was conducted using computational resources at the Maryland Advanced Research Computing Center (MARCC). We acknowledge the use of the Legacy Archive for Microwave Background Data Analysis (LAMBDA), part of the High Energy Astrophysics Science Archive Center (HEASARC). HEASARC/LAMBDA is a service of the Astrophysics Science Division at the NASA Goddard Space Flight Center. NF is supported by Fundação para a Ciência e a Tecnologia (FCT) through the research grants UIDB/04434/2020, UIDP/04434/2020, PTDC/FIS-OUT/29048/2017, CERN/FIS-PAR/0037/2019 and the personal research FCT grant “CosmoTests – Cosmological tests of gravity theories beyond General Relativity” with ref. number CEECIND/00017/2018. The work of ADF was supported by Japan Society for the Promotion of Science (JSPS) Grants-in-Aid for Scientific Research No. 20K03969. ST is supported by the Grant-in-Aid for Scientific Research Fund of the JSPS No. 19K03854.

-
- [1] A. G. Riess *et al.* (Supernova Search Team), *Astron. J.* **116**, 1009 (1998), arXiv:astro-ph/9805201.
 - [2] S. Perlmutter *et al.* (Supernova Cosmology Project), *Astrophys. J.* **517**, 565 (1999), arXiv:astro-ph/9812133.
 - [3] D. N. Spergel *et al.* (WMAP), *Astrophys. J. Suppl.* **148**, 175 (2003), arXiv:astro-ph/0302209.
 - [4] P. A. R. Ade *et al.* (Planck), *Astron. Astrophys.* **571**, A16 (2014), arXiv:1303.5076 [astro-ph.CO].
 - [5] D. J. Eisenstein *et al.* (SDSS), *Astrophys. J.* **633**, 560 (2005), arXiv:astro-ph/0501171.
 - [6] S. Weinberg, *Rev. Mod. Phys.* **61**, 1 (1989).
 - [7] V. Sahni and A. Starobinsky, *International Journal of Modern Physics D* **9**, 373 (2000), arXiv:astro-ph/9904398 [astro-ph].
 - [8] P. J. E. Peebles and B. Ratra, *Rev. Mod. Phys.* **75**, 559 (2003), arXiv:astro-ph/0207347.
 - [9] P. A. Zyla *et al.*, *Progress of Theoretical and Experimental Physics* **2020**, 083C01 (2020).
 - [10] R. H. Cyburt, B. D. Fields, K. A. Olive, and T.-H. Yeh, *Reviews of Modern Physics* **88**, 015004 (2016), arXiv:1505.01076 [astro-ph.CO].
 - [11] D. M. Scolnic *et al.*, *Astrophys. J.* **859**, 101 (2018), arXiv:1710.00845 [astro-ph.CO].
 - [12] S. Alam *et al.*, *Phys. Rev. D* **103**, 083533 (2021), arXiv:2007.08991 [astro-ph.CO].
 - [13] J. Martin, *Comptes Rendus Physique* **13**, 566 (2012), arXiv:1205.3365 [astro-ph.CO].
 - [14] A. Joyce, B. Jain, J. Khoury, and M. Trodden, *Phys. Rept.* **568**, 1 (2015), arXiv:1407.0059 [astro-ph.CO].
 - [15] A. Padilla, (2015), arXiv:1502.05296 [hep-th].
 - [16] N. Aghanim *et al.* (Planck), (2018), arXiv:1807.06209 [astro-ph.CO].
 - [17] A. G. Riess, S. Casertano, W. Yuan, J. B. Bowers, L. Macri, J. C. Zinn, and D. Scolnic, **908**, L6 (2021).
 - [18] L. Knox and M. Millea, *Phys. Rev. D* **101**, 043533 (2020), arXiv:1908.03663 [astro-ph.CO].
 - [19] A. G. Riess, *Nature Reviews Physics* **2**, 10 (2020), arXiv:2001.03624 [astro-ph.CO].
 - [20] H. Hildebrandt *et al.*, *A & A* **633**, A69 (2020), arXiv:1812.06076 [astro-ph.CO].
 - [21] S. Joudaki *et al.*, *MNRAS* **474**, 4894 (2018), arXiv:1707.06627 [astro-ph.CO].
 - [22] C. Hikage *et al.*, *PASJ* **71**, 43 (2019), arXiv:1809.09148 [astro-ph.CO].
 - [23] T. M. C. Abbott *et al.* (DES), arXiv e-prints (2021), arXiv:2105.13549 [astro-ph.CO].
 - [24] C. Heymans *et al.*, *A & A* **646**, A140 (2021), arXiv:2007.15632 [astro-ph.CO].

- [25] P. Bull *et al.*, Physics of the Dark Universe **12**, 56 (2016), arXiv:1512.05356 [astro-ph.CO].
- [26] E. Di Valentino, O. Mena, S. Pan, L. Visinelli, W. Yang, A. Melchiorri, D. F. Mota, A. G. Riess, and J. Silk, Classical and Quantum Gravity **38**, 153001 (2021), arXiv:2103.01183 [astro-ph.CO].
- [27] N. Schöneberg, G. F. Abellán, A. Pérez Sánchez, S. J. Witte, c. V. Poulin, and J. Lesgourgues, arXiv e-prints, arXiv:2107.10291 (2021), arXiv:2107.10291 [astro-ph.CO].
- [28] E. J. Copeland, M. Sami, and S. Tsujikawa, Int. J. Mod. Phys. **D15**, 1753 (2006), arXiv:hep-th/0603057 [hep-th].
- [29] J. Martin, Mod. Phys. Lett. A **23**, 1252 (2008), arXiv:0803.4076 [astro-ph].
- [30] S. Tsujikawa, Classical and Quantum Gravity **30**, 214003 (2013), arXiv:1304.1961 [gr-qc].
- [31] T. Chiba, A. De Felice, and S. Tsujikawa, Phys. Rev. D **87**, 083505 (2013), arXiv:1210.3859 [astro-ph.CO].
- [32] J.-B. Durrive, J. Ooba, K. Ichiki, and N. Sugiyama, Phys. Rev. D **97**, 043503 (2018), arXiv:1801.09446 [astro-ph.CO].
- [33] A. Banerjee, H. Cai, L. Heisenberg, E. Ó. Colgáin, M. M. Sheikh-Jabbari, and T. Yang, Phys. Rev. D **103**, L081305 (2021), arXiv:2006.00244 [astro-ph.CO].
- [34] D. Lovelock, J. Math. Phys. **12**, 498 (1971).
- [35] D. Lovelock, J. Math. Phys. **13**, 874 (1972).
- [36] B. Boisseau, G. Esposito-Farese, D. Polarski, and A. A. Starobinsky, Phys. Rev. Lett. **85**, 2236 (2000), arXiv:gr-qc/0001066.
- [37] A. Lue, R. Scoccimarro, and G. D. Starkman, Phys. Rev. **D69**, 124015 (2004), arXiv:astro-ph/0401515 [astro-ph].
- [38] A. Silvestri and M. Trodden, Rept. Prog. Phys. **72**, 096901 (2009), arXiv:0904.0024 [astro-ph.CO].
- [39] S. Nojiri and S. D. Odintsov, Phys. Rept. **505**, 59 (2011), arXiv:1011.0544 [gr-qc].
- [40] S. Tsujikawa, Lect. Notes Phys. **800**, 99 (2010), arXiv:1101.0191 [gr-qc].
- [41] S. Capozziello and M. De Laurentis, Phys. Rept. **509**, 167 (2011), arXiv:1108.6266 [gr-qc].
- [42] T. Clifton, P. G. Ferreira, A. Padilla, and C. Skordis, Phys. Rept. **513**, 1 (2012), arXiv:1106.2476 [astro-ph.CO].
- [43] K. Bamba, S. Capozziello, S. Nojiri, and S. D. Odintsov, Astrophys. Space Sci. **342**, 155 (2012), arXiv:1205.3421 [gr-qc].
- [44] K. Koyama, Rept. Prog. Phys. **79**, 046902 (2016), arXiv:1504.04623 [astro-ph.CO].
- [45] P. Avelino *et al.*, Symmetry **8**, 70 (2016), arXiv:1607.02979 [astro-ph.CO].
- [46] A. Joyce, L. Lombriser, and F. Schmidt, Ann. Rev. Nucl. Part. Sci. **66**, 95 (2016), arXiv:1601.06133 [astro-ph.CO].
- [47] S. Nojiri, S. D. Odintsov, and V. K. Oikonomou, Phys. Rept. **692**, 1 (2017), arXiv:1705.11098 [gr-qc].
- [48] R. Kase and S. Tsujikawa, Phys. Rev. **D97**, 103501 (2018), arXiv:1802.02728 [gr-qc].
- [49] P. G. Ferreira, Ann. Rev. Astron. Astrophys. **57**, 335 (2019), arXiv:1902.10503 [astro-ph.CO].
- [50] T. Kobayashi, Rept. Prog. Phys. **82**, 086901 (2019), arXiv:1901.07183 [gr-qc].
- [51] N. Frusciante and L. Perenon, Phys. Rept. **857**, 1 (2020), arXiv:1907.03150 [astro-ph.CO].
- [52] E. N. Saridakis *et al.* (CANTATA), (2021), arXiv:2105.12582 [gr-qc].
- [53] G. W. Horndeski, Int. J. Theor. Phys. **10**, 363 (1974).
- [54] C. Deffayet, X. Gao, D. A. Steer, and G. Zahariade, Phys. Rev. **D84**, 064039 (2011), arXiv:1103.3260 [hep-th].
- [55] T. Kobayashi, M. Yamaguchi, and J. Yokoyama, Prog. Theor. Phys. **126**, 511 (2011), arXiv:1105.5723 [hep-th].
- [56] C. Charmousis, E. J. Copeland, A. Padilla, and P. M. Saffin, Phys. Rev. Lett. **108**, 051101 (2012), arXiv:1106.2000 [hep-th].
- [57] B. P. Abbott *et al.* (LIGO Scientific, Virgo), Phys. Rev. Lett. **119**, 161101 (2017), arXiv:1710.05832 [gr-qc].
- [58] A. De Felice and S. Tsujikawa, JCAP **1202**, 007 (2012), arXiv:1110.3878 [gr-qc].
- [59] C. Deffayet, O. Pujolas, I. Sawicki, and A. Vikman, JCAP **1010**, 026 (2010), arXiv:1008.0048 [hep-th].
- [60] C. Deffayet, G. Esposito-Farese, and A. Vikman, Phys. Rev. **D79**, 084003 (2009), arXiv:0901.1314 [hep-th].
- [61] S. Nesseris, A. De Felice, and S. Tsujikawa, Phys. Rev. D **82**, 124054 (2010), arXiv:1010.0407 [astro-ph.CO].
- [62] J. Renk, M. Zumalacarregui, F. Montanari, and A. Barreira, JCAP **1710**, 020 (2017), arXiv:1707.02263 [astro-ph.CO].
- [63] S. Peirone, N. Frusciante, B. Hu, M. Raveri, and A. Silvestri, Phys. Rev. **D97**, 063518 (2018), arXiv:1711.04760 [astro-ph.CO].
- [64] S. Peirone, G. Benevento, N. Frusciante, and S. Tsujikawa, (2019), arXiv:1905.05166 [astro-ph.CO].
- [65] N. Frusciante, S. Peirone, L. Atayde, and A. De Felice, Phys. Rev. D **101**, 064001 (2020), arXiv:1912.07586 [astro-ph.CO].
- [66] A. De Felice and S. Tsujikawa, JCAP **1203**, 025 (2012), arXiv:1112.1774 [astro-ph.CO].
- [67] P. Brax and P. Valageas, Phys. Rev. D **90**, 023507 (2014), arXiv:1403.5420 [astro-ph.CO].
- [68] P. Brax, C. Burrage, and A.-C. Davis, JCAP **1603**, 004 (2016), arXiv:1510.03701 [gr-qc].
- [69] P. Brax and P. Valageas, Journal of Cosmology and Astroparticle Physics **2016**, 020–020 (2016).
- [70] J. Khoury and A. Weltman, Phys. Rev. Lett. **93**, 171104 (2004), arXiv:astro-ph/0309300 [astro-ph].
- [71] A. I. Vainshtein, Phys. Lett. **B39**, 393 (1972).
- [72] T. Chiba, T. Okabe, and M. Yamaguchi, Phys. Rev. D **62**, 023511 (2000), arXiv:astro-ph/9912463.
- [73] C. Armendariz-Picon, V. F. Mukhanov, and P. J. Steinhardt, Phys. Rev. Lett. **85**, 4438 (2000), arXiv:astro-ph/0004134.
- [74] A. De Felice, T. Kobayashi, and S. Tsujikawa, Phys. Lett. **B706**, 123 (2011), arXiv:1108.4242 [gr-qc].
- [75] R. Kase and S. Tsujikawa, Int. J. Mod. Phys. D **28**, 1942005 (2019), arXiv:1809.08735 [gr-qc].
- [76] L. Amendola, M. Kunz, and D. Sapone, JCAP **0804**, 013 (2008), arXiv:0704.2421 [astro-ph].
- [77] R. Bean and M. Tangmatitham, Phys. Rev. **D81**, 083534 (2010), arXiv:1002.4197 [astro-ph.CO].
- [78] A. Silvestri, L. Pogosian, and R. V. Buniy, Phys. Rev. **D87**, 104015 (2013), arXiv:1302.1193 [astro-ph.CO].
- [79] L. Amendola, D. Bettoni, A. M. Pinho, and S. Casas, Universe **6**, 20 (2020), arXiv:1902.06978 [astro-ph.CO].
- [80] V. Acquaviva and C. Baccigalupi, Phys. Rev. D **74**, 103510 (2006), arXiv:astro-ph/0507644.
- [81] C. Carbone, M. Baldi, V. Pettorino, and C. Baccigalupi, JCAP **09**, 004 (2013), arXiv:1305.0829 [astro-ph.CO].

- [82] R. K. Sachs and A. M. Wolfe, *Astrophys. J.* **147**, 73 (1967).
- [83] L. Kofman and A. A. Starobinsky, *Sov. Astron. Lett.* **11**, 271 (1985).
- [84] T. Giannantonio, R. Scranton, R. G. Crittenden, R. C. Nichol, S. P. Boughn, A. D. Myers, and G. T. Richards, *Phys. Rev. D* **77**, 123520 (2008), arXiv:0801.4380 [astro-ph].
- [85] S. P. Boughn, R. G. Crittenden, and N. G. Turok, *New Astron.* **3**, 275 (1998), arXiv:astro-ph/9704043 [astro-ph].
- [86] S. P. Boughn and R. G. Crittenden, *Phys. Rev. Lett.* **88**, 021302 (2001), arXiv:astro-ph/0111281 [astro-ph].
- [87] B. Stözlner, A. Cuoco, J. Lesgourgues, and M. Bilicki, *Phys. Rev. D* **97**, 063506 (2018), arXiv:1710.03238 [astro-ph.CO].
- [88] Y.-S. Song, W. Hu, and I. Sawicki, *Phys. Rev. D* **75**, 044004 (2007), arXiv:astro-ph/0610532 [astro-ph].
- [89] A. Barreira, B. Li, C. M. Baugh, and S. Pascoli, *Phys. Rev. D* **86**, 124016 (2012), arXiv:1208.0600 [astro-ph.CO].
- [90] F. Giacomello, A. De Felice, and S. Ansoldi, *JCAP* **1903**, 038 (2019), arXiv:1811.10885 [astro-ph.CO].
- [91] Q. Hang, S. Alam, Y.-C. Cai, and J. A. Peacock, *MNRAS* **507**, 510 (2021), arXiv:2105.11936 [astro-ph.CO].
- [92] R. Scranton, A. J. Connolly, R. C. Nichol, A. Stebbins, I. Szapudi, D. J. Eisenstein, N. Afshordi, T. Budavari, I. Csabai, J. A. Frieman, J. E. Gunn, D. Johnston, Y. Loh, R. H. Lupton, C. J. Miller, E. S. Sheldon, R. S. Sheth, A. S. Szalay, M. Tegmark, and Y. Xu, arXiv e-prints, astro-ph/0307335 (2003), arXiv:astro-ph/0307335 [astro-ph].
- [93] U. Sawangwit, T. Shanks, R. D. Cannon, S. M. Croom, N. P. Ross, and D. A. Wake, *MNRAS* **402**, 2228 (2010), arXiv:0911.1352 [astro-ph.CO].
- [94] C. L. Francis and J. A. Peacock, *MNRAS* **406**, 2 (2010), arXiv:0909.2494 [astro-ph.CO].
- [95] Q. Hang, S. Alam, J. A. Peacock, and Y.-C. Cai, *MNRAS* **501**, 1481 (2021), arXiv:2010.00466 [astro-ph.CO].
- [96] A. Krolewski and S. Ferraro, arXiv e-prints, arXiv:2110.13959 (2021), arXiv:2110.13959 [astro-ph.CO].
- [97] R. Kimura, T. Kobayashi, and K. Yamamoto, *Phys. Rev. D* **85**, 123503 (2012), arXiv:1110.3598 [astro-ph.CO].
- [98] S. Nakamura, A. De Felice, R. Kase, and S. Tsujikawa, *Phys. Rev. D* **99**, 063533 (2019), arXiv:1811.07541 [astro-ph.CO].
- [99] E. Bertschinger and P. Zukin, *Phys. Rev. D* **78**, 024015 (2008), arXiv:0801.2431 [astro-ph].
- [100] L. Pogosian, A. Silvestri, K. Koyama, and G.-B. Zhao, *Phys. Rev. D* **81**, 104023 (2010), arXiv:1002.2382 [astro-ph.CO].
- [101] S. Tsujikawa, *Phys. Rev. D* **76**, 023514 (2007), arXiv:0705.1032 [astro-ph].
- [102] I. Sawicki and E. Bellini, *Phys. Rev. D* **92**, 084061 (2015), arXiv:1503.06831 [astro-ph.CO].
- [103] S. Peirone, K. Koyama, L. Pogosian, M. Raveri, and A. Silvestri, *Phys. Rev. D* **97**, 043519 (2018), arXiv:1712.00444 [astro-ph.CO].
- [104] N. Frusciante, S. Peirone, S. Casas, and N. A. Lima, *Phys. Rev. D* **99**, 063538 (2019), arXiv:1810.10521 [astro-ph.CO].
- [105] N. Frusciante and F. Pace, *Phys. Dark Univ.* **30**, 100686 (2020), arXiv:2004.11881 [astro-ph.CO].
- [106] G. Benevento, M. Raveri, A. Lazanu, N. Bartolo, M. Liguori, P. Brax, and P. Valageas, *JCAP* **05**, 027 (2019), arXiv:1809.09958 [astro-ph.CO].
- [107] B. Hu, M. Raveri, N. Frusciante, and A. Silvestri, *Phys. Rev. D* **89**, 103530 (2014), arXiv:1312.5742 [astro-ph.CO].
- [108] M. Raveri, B. Hu, N. Frusciante, and A. Silvestri, *Phys. Rev. D* **90**, 043513 (2014), arXiv:1405.1022 [astro-ph.CO].
- [109] B. Hu, M. Raveri, N. Frusciante, and A. Silvestri, (2014), arXiv:1405.3590 [astro-ph.IM].
- [110] G. Gubitosi, F. Piazza, and F. Vernizzi, *JCAP* **1302**, 032 (2013), [JCAP1302.032(2013)], arXiv:1210.0201 [hep-th].
- [111] J. K. Bloomfield, E. E. Flanagan, M. Park, and S. Watson, *JCAP* **1308**, 010 (2013), arXiv:1211.7054 [astro-ph.CO].
- [112] R. Kase and S. Tsujikawa, *Int. J. Mod. Phys. D* **23**, 1443008 (2015), arXiv:1409.1984 [hep-th].
- [113] A. Challinor and A. Lewis, *Phys. Rev. D* **84**, 043516 (2011), arXiv:1105.5292 [astro-ph.CO].
- [114] J. Bloomfield, *JCAP* **1312**, 044 (2013), arXiv:1304.6712 [astro-ph.CO].
- [115] J. Gleyzes, D. Langlois, F. Piazza, and F. Vernizzi, *JCAP* **1308**, 025 (2013), arXiv:1304.4840 [hep-th].
- [116] J. Gleyzes, D. Langlois, and F. Vernizzi, *Int. J. Mod. Phys. D* **23**, 1443010 (2015), arXiv:1411.3712 [hep-th].
- [117] N. Frusciante, M. Raveri, D. Vernieri, B. Hu, and A. Silvestri, *Phys. Dark Univ.* **13**, 7 (2016), arXiv:1508.01787 [astro-ph.CO].
- [118] N. Frusciante, G. Papadomanolakis, and A. Silvestri, *JCAP* **1607**, 018 (2016), arXiv:1601.04064 [gr-qc].
- [119] S. Peirone, G. Benevento, N. Frusciante, and S. Tsujikawa, *Phys. Rev. D* **100**, 063509 (2019), arXiv:1905.11364 [astro-ph.CO].
- [120] Planck Collaboration, P. A. R. Ade, and others, *Astronomy and Astrophysics* **594**, A13 (2016).
- [121] M. Bilicki, T. H. Jarrett, J. A. Peacock, M. E. Cluver, and L. Steward, *ApJs* **210**, 9 (2014), arXiv:1311.5246 [astro-ph.CO].
- [122] D. Alonso, A. I. Salvador, F. J. Sánchez, M. Bilicki, J. García-Bellido, and E. Sánchez, *MNRAS* **449**, 670 (2015), arXiv:1412.5151 [astro-ph.CO].
- [123] M. Bilicki, J. A. Peacock, T. H. Jarrett, M. E. Cluver, N. Maddox, M. J. I. Brown, E. N. Taylor, N. C. Hambly, A. Solarz, B. W. Holwerda, I. Baldry, J. Loveday, A. Moffett, A. M. Hopkins, S. P. Driver, M. Alpaslan, and J. Bland-Hawthorn, *ApJs* **225**, 5 (2016), arXiv:1607.01182 [astro-ph.CO].
- [124] R. Beck, L. Dobos, T. Budavári, A. S. Szalay, and I. Csabai, *MNRAS* **460**, 1371 (2016), arXiv:1603.09708 [astro-ph.GA].
- [125] G. T. Richards, A. D. Myers, A. G. Gray, R. N. Riegel, R. C. Nichol, R. J. Brunner, A. S. Szalay, D. P. Schneider, and S. F. Anderson, *ApJs* **180**, 67 (2009), arXiv:0809.3952 [astro-ph].
- [126] J. J. Condon, W. D. Cotton, E. W. Greisen, Q. F. Yin, R. A. Perley, G. B. Taylor, and J. J. Broderick, *The Astronomical Journal* **115**, 1693 (1998).
- [127] N. Aghanim *et al.* (Planck), (2019), arXiv:1907.12875 [astro-ph.CO].
- [128] S. Alam *et al.* (BOSS), *Mon. Not. Roy. Astron. Soc.* **470**, 2617 (2017), arXiv:1607.03155 [astro-ph.CO].
- [129] A. J. Ross, L. Samushia, C. Howlett, W. J. Percival, A. Burden, and M. Manera, *mnras* **449**, 835 (2015), arXiv:1409.3242.
- [130] F. Beutler, C. Blake, M. Colless, D. H. Jones, L. Staveley-Smith, L. Campbell, Q. Parker, W. Saunders, and F. Watson, *mnras* **416**, 3017 (2011), arXiv:1106.3366.
- [131] P. A. R. Ade *et al.* (Planck), *Astron. Astrophys.* **594**, A15 (2016), arXiv:1502.01591 [astro-ph.CO].